Amphiphili Nano-Swords for Direct Penetration and Eradiation of Pathogenic Bacterial Bioflms

Cailing Zhou, [a] # Yu Zhou, [a] # Yaqian Zheng,[b] Yue Yu, [a] Kailing Yang,[a] Zhiyong Chen,[a] Xianhui Chen,[a] Kang Wen,[a] Yajie Chen,[a] Silei Bai,[a] Junfeng Song,[a] Tong Wu,[a] E Lei,[a] Muyang Wan [d], Luyan Z. Ma, [b] * Wing-Leung Wong, [c] * Yugang Bai, [a] * Chunhui Zhang, [d] * and Xinxin Feng [a] *

# These authors contributed equally to this work.

[a] C. Zhou, Y. Zhou, K. Yang, Z. Chen, X. Chen, K. Wen, Y. Chen, S. Bai, J. Song, T. Wu, E. Lei, Y. Bai, X. Feng
Institute of Chemical Biology and Nanomedicine, State Key Laboratory of Chemo/Biosensing and Chemometrics, Hunan Provincial Key Laboratory of Biomacromolecular Chemical Biology, and School of Chemistry and Chemical Engineering, Hunan University, Changsha, Hunan, 410082, China
E-mail: baiyugang@hnu.edu.cn; xinxin_feng@hnu.edu.cn

[b] Y. Zheng, L. Z. Ma
State Key Laboratory of Microbial Resources, Institute of Microbiology, Chinese Academy of Sciences, Beijing, China
E-mail: luyanma27@im.ac.cn

[c] W.-L. Wong
State Key Laboratory of Chemical Biology and Drug Discovery, Department of Applied Biology and Chemical Technology, The Hong Kong Polytechnic University, Hung Hom, Kowloon, Hong Kong SAR, China.
E-mail: wing.leung.wong@polyu.edu.hk

[d] C. Zhang
School of Biology, Hunan University, Changsha, Hunan, 410082, China
E-mail: chzhang@hnu.edu.cn

* Corresponding author

ABSTRACT:

Bacterial biofilms are major causes of persistent and recurrent infections and implant failures. Biofilms are formable by most clinically important pathogens worldwide, such as *Staphylococcus aureus*, *Pseudomonas aeruginosa*, and *Escherichia coli*, causing recalcitrance to standard antibiotic therapy or anti-biofilm strategies due to amphiphilic impermeable extracellular polymeric substances (EPS) and the presence of resistant and persistent bacteria within the biofilm matrix. Herein, we report our design of an oligoamidine-based amphiphilic "nano-sword" with high structural compacity and rigidity. Its rigid, amphiphilic structure ensures effective penetration into EPS, and the membrane-DNA dual-targeting mechanism exerts strong bactericidal effect on the dormant bacterial persisters within biofilms. The potency of this oligoamidine is shown in two distinct modes of application: it may be used as a coating agent for polycaprolactone to fully inhibit surface biofilm growth in an implant-site mimicking micro-environment; meanwhile, it cures model mice of biofilm infections in various *ex vivo* and *in vivo* studies.

KEYWORDS:

Anti-bacterial biofilm; Amphiphilic oligomers; Extracellular polymeric substance; Persister cells

INTRODUCTION

Bacteria exist in two different forms, planktonic state (free floating) and biofilm (adhered to a surface), both of which have existed on the earth since the first bacteria evolved.[1] While planktonic bacteria are generally sensitive to antibiotics, biofilm is highly resistant. Therefore, biofilms formed by pathogenic bacteria are recognized as the roots of many persistent infectious diseases. The U.S. National Institutes of Health (NIH) revealed that bacterial biofilms contribute to 65 and 80% of microbial and chronic infections,[2] respectively, as well as to a major portion of implantable device-related infections.[3] The recalcitrance of biofilm to medical treatment is largely due to their intrinsic tolerance to conventional antibiotics and host immune response, a trait endowed by its two major structural and sub-populational features,[4] namely, the matrix of extracellular polymeric substances (EPS) and the presence of resistant, dormant, and persistent bacteria within the biofilm matrix. EPS forms a highly impermeable amphiphilic protective layer for the residing bacterial communities. The surface of EPS is coated with a hydrophobic layer composed mostly of proteins such as hydrophobin and amyloid [5−13] (Figure 1A). Inside the EPS matrix is a highly hydrophilic environment containing extensively entangled eDNA, proteins, and polysaccharides, as well as water channels and pores that transport and store nutrients.[14,15] Such structure results in high impermeability to a broad range of chemicals including antibiotics. In addition, embedded in the EPS are heterogenous populations of active, dormant, and persistent bacteria cells (Figure 1A). Dormant persister cells are metabolically inactive, invalidating many antibiotics whose antimicrobial mechanisms of action are growth-dependent. Collectively, formation of biofilm results in 10−1000 times more antibiotic resistance than the corresponding planktonic bacteria,[4,16] meanwhile accounting for the recalcitrance and relapsing nature of such infections *in vivo*.[17]

Current anti-biofilm strategies, such as targeting EPS chemical components for integrity compromise, inhibiting EPS synthesis and secretion, and interfering with metabolic activity or direct killing of dormant cells, offer some clinical promise for biofilm inhibition.[18] However, eradication of established biofilms remains a challenge and thus attracts much research interest.[19−26] This is presumably because the agents' penetration into the amphiphilic EPS is highly restricted. Therefore, development of an anti-biofilm agent with high biofilm permeability by targeting the densely packed and amphiphilic structure of EPS is in urgent demand.

An easy and effective strategy to penetrate, and possibly also disrupt an amphiphilic structure at the same time, is to use an amphiphilic molecule with reversed charge states. For a well-known example, cationic surfactants, such as cetrimonium bromide (a C16 quaternary ammonium surfactant), can easily kill cells by disrupting their membrane composed of an anionically amphiphilic lipid bilayer.[27] Therefore, one may expect the use of a cationic amphiphilic structure to facilitate EPS penetration and disruption as EPS layers are also anionically amphiphilic due to the polyanionic nature of extracellular DNA and polysaccharides.[28] In addition to the consideration of surface charge properties, the size and shape of the anti-biofilm agents also have profound impact on their ability to penetrate the densely packed EPS. For example, nitric oxide-releasing particles with a decreased size and increased aspect ratio (rod-like shape) were proved to be more effective in delivering NO and inducing greater antibacterial action throughout the bacterial biofilm.[29] Therefore, a rod-like structure with some degree of rigidity (analogous to a "nanosword") is a preferred molecular design.

Antimicrobial peptides and macromolecules are promising scaffolds in achieving antimicrobial and anti-biofilm effects,[30 – 38] with diverse functional tunability for different application purposes, such as selective targeting moiety, smart delivery, antibiotic adjuvants, surface functionalization, etc., and at the same time possess high biocompatibility. We have previously reported a series of oligoamidine-based peptidomimetics (i.e., short synthetic polymers mimicking the structure, function, or mechanics of polypeptides) with dual membrane/DNA targeting mechanism as effective antimicrobial agents.[39] The amidine arrays promote bacterial DNA binding as a secondary non-growth-dependent mechanism of action, which endows those oligoamidines with resistance-resistant nature. Our previous studies also indicate that structural adjustments on such dual-mechanistic peptidomimetics give rod-like topologies that significantly affect their selectivity and potency.[40−42] Therefore, we speculated that this known information may also be helpful in finding a viable antibiofilm agent and hoped to find the contributing factors for biofilm eradication within this oligoamidine platform. With these considerations, we report an alternate amphiphilic oligoamidine with a rigid structure as an effective anti-biofilm agent that may provide these desirable merits with limited toxicity concerns (Figure 1B). The oligomer's "sword"-like amphiphilic topology and its extra, DNA-based mechanism of action ensure its potency toward the EPS layer and dormant bacteria, while its harm to eukaryotic cells is minimized (Figure 1C). The effectiveness of this oligoamidine was evaluated with biofilms of *Staphylococcus aureus* (*S. aureus*), *Escherichia coli* (*E. coli*), and *Pseudomonas aeruginosa* (*P. aeruginosa*) in several *ex-vivo* and *in vivo* models.

RESULTS AND DISCUSSION

Exploring the Structure−Activity Relationship of Oligoamidine against Biofilm.

Oligoamidines **3a−i** were synthesized from *p*-ethylphthalimidate (**1**) and various diamines (**2a−i**) (Figures 2A and S1−S11) of different hydrophobicity, flexibility, and atomic spatial density, which are factors known to impact the capability of penetration into bacterial biofilms.[29,43] These compounds have generally good solubility in water without self-assembling (Figure S12). **3a−i** were first tested for their antimicrobial activities, finding similar minimum inhibitory concentrations (MICs, 0.25−2 μg/mL) against *S. aureus* (Figure S13). **3a−i** were then evaluated using a biofilm growth inhibition assay against *S. aureus*, a biofilm formed with high clinical importance [44] to give their minimum biofilm inhibition concentrations (MBICs). The MBIC values indicate that, **3a**, the oligomer with a *meta*-substituted phenylene diamine linker (**2a**), was found to have the best activity (MBIC = 16 μg/mL), followed by **3b** (with linker **2b**, a *para*-substituted analog of **2a**) and **3c** (with linker **2c**, a highly branched structure) with MBIC = 32 μg/mL (Figure 2A). In addition, it was found that the oligoamidines **3d−i** with more flexible linkers tend to have weaker anti-biofilm activities (MBICs = 64∼128 μg/mL). In addition, there is no apparent association between antimicrobial/anti-biofilm activities and hemolytic/cell growth toxicities (Figure S13), and **3a** possesses the highest therapeutic index and thus was selected as the hit compound for following studies.

To further identify potential structural rules that govern the potency of biofilm inhibition, we carried out a quantitative examination of the above structure − activity relationship (SAR) analysis by adopting a molecular descriptor-based approach.[45,46] Molecular characteristics of the nine diamines were computed with regard to multiple features: physical properties, atom and bond counts, conformation-dependent charge properties, partial charge configurations, pharmacophore features, potential energy

descriptors, number of 3D conformations, adjacency and distance matrix descriptors, and Kier and Hall connectivity and kappa shape indices (SI Excel file). The MBIC values of the oligoamidines were plotted against every descriptor from the above categories (Figure S14A), and the rank-ordered Pearson's R values from a least square fit model are shown in Figure 2B and Table S1. It was found that the top nine descriptors generally represent three important molecular characteristics, resulting in an increased anti-biofilm activity of oligomers: higher hydrophobicity (log*P*(*o*/*w*), PEPE_VSA_FHYD, a_donacc, lip_acc, and ASA_P), higher structural compacity (Kier2, diameter), and higher structural rigidity (E_tor, number of possible conformations). All these characteristics are consistent with the linker structure of **3a**, which has a rigid and rod-shaped "sword"-like amphiphilic topology with alternating amidines and rigid/compact aromatic linkers. **3a** was thus chosen as our lead compound in this study, and its antimicrobial activities against different pathogens were determined, with minimum inhibitory concentrations (MICs) ranging from 0.5 to 2 μg/mL against clinically critical pathogenic bacteria (*S. aureus*, *E. coli*, *K. pneumoniae*, *A. baumannii*, *Enterobacter cloacae*, and *P. aeruginosa*) in the planktonic state (Figure S14B). The results clearly indicated that the compound was potent and broad-spectrum.

3a Is Effective in the Inhibition and Eradication of Various Pathogenic Bacterial Biofilms.

Clinically important pathogens, such as *S. aureus*, *P. aeruginosa*, and *E. coli*,[47−49] may form biofilms upon infection on tissues or implanted devices within hours,[50] becoming major causes of persistent and recurrent infections. Therefore, for successful biofilm remediation, the agent of choice should be capable of inhibiting biofilm formation at the early stage (Figure 3A-i) and eradicating mature biofilms by disrupting the biofilm cell community (Figure 3A-ii). We have demonstrated the ability of **3a** in inhibiting *S. aureus* biofilm formation in the SAR study (Figure 2A, MBIC = 16 μg/mL), and in continued explorations, we found the compound even more potent (8 μg/mL) for the inhibition of *P. aeruginosa* and *E. coli* biofilm formation (Figure 3B). More importantly, the potency of **3a** was less hindered by mature biofilms at a higher concentration, and such hindrance has been the primary issue for most antimicrobial agents. **3a** was able to completely eradicate mature biofilms at a higher concentration, with minimum biofilm eradication concentrations (MBECs) of 64 μg/mL (against *S. aureus* biofilm), 256 μg/mL (against *P. aeruginosa* biofilm), and 128 μg/mL (against *E. coli* biofilm), as quantified in Figure 3C and imaged in Figure 3D with a GFP-harboring strain of *S. aureus* (GFP-*S. aureus*). Using 3D confocal scanning of GFP-*S. a*, the biomass of living bacteria in biofilm formed in 24 h was observed to be 11.7 $\mu m^3/\mu m^2$. Treatment with 32 or 64 μg/mL **3a** reduces the biofilm biomass to 2∼3 $\mu m^3/\mu m^2$, with clearly noticeable increase of dead bacteria (stained with propidium iodide, Figures 3D, S15, and Movies 1, 2, and 3). Quantitative analysis in Figure 3E,F also suggests that such biomass reduction of living bacteria in biofilm and increase of dead bacteria cell numbers are significant.

The antibiofilm behavior is thus in sharp contrast with the antimicrobial and anti-biofilm behavior of a standard antibiotic, vancomycin, which has an ultra-potent MIC against *S. aureus* (0.5 μg/mL) and adequate MBIC (4 μg/mL, Figure S16A) but fails to eradicate the mature *S. aureus* biofilm even at a concentration of 1024 μg/mL (Figure S16B). The deactivation of vancomycin against *S. aureus* biofilm (Figure 3G, vancomycin) is a typical demonstration of biofilm's intrinsic impermeability to small molecules with its amphiphilic and densely packed EPS, plus its reduced susceptibility to clinical antibiotics resulting from a heterogenous

bacterial population. In contrast, **3a** maintained much higher biofilm eradication activity (Figure 3G, **3a**) due to its rigid alternatingly amphiphilic structure and dual-targeting antimicrobial mechanisms, which facilitate disruption of EPS and endow its nongrowth-dependent bactericidal activity.

3a Disrupts the Biofilm Cell Community and Kills Bacteria with Different Lifestyles.

We believe that the biofilm eradication ability of **3a** stems from its ability in penetrating the amphiphilic and densely packed EPS, allowing direct disruption of the biofilm cell community. This assumption is supported by biofilm morphology images captured using scanning electron microscopy (SEM). As shown in Figure 4A, the treatment of **3a** resulted in dispersion of EPS and isolation of individual bacterial cells. On the contrary, vancomycin has no effect on the biofilm matrix. In addition, the morphology of biofilm bacterial cells treated with **3a** was found altered significantly compared to normal cells. They featured a markedly reduced diameter and damaged cell membrane, suggesting a strong bactericidal effect. As previously mentioned, biofilm harbors bacterial cells with diverse lifestyles including active cells, dormant cells, and persistent cells.[51] We determined the minimum inhibitory concentration of **3a** against actively growing *S. aureus* (initial concentration of 5×10^5 CFU/mL) to be 4 μg/mL, which was weaker than that of vancomycin (1 μg/mL, Figure 4B). However, when dormancy was induced by culturing the cells in a nutrient-deficient medium (DMEM-10% FBS) that limited bacterial growth,[52] the minimum bactericidal concentration of **3a** was reduced to 0.5 μg/mL, 16 times better than that of vancomycin (8 μg/mL) (Figure 4C). The increased bactericidal activity of **3a** is presumably due to the significantly inhibited self-healing ability (on membrane and DNA damage) of bacteria in the dormant state, plus the invulnerability of its non-growth-relating working mechanism to dormancy. In contrast, vancomycin, which targets cell wall biosynthesis,[53] was largely deactivated, as biosynthetic and metabolic activities in dormant bacteria were significantly reduced.

Besides dormant cells, persisters are also produced in biofilms and confer multidrug tolerance to almost all known antimicrobials.[51] Under in vitro conditions, persister cells can be selected and enriched by the treatment with a high concentration of antibiotics.[52,54] Thus, a population of highly persistent *S. aureus* cells was generated with vancomycin at its 10X MIC for a 6 h treatment (Figure 4D). After that, different concentrations of **3a** were added. With **3a** at 32 μg/mL, all persister cells (with 8 log CFU) were sterilized within 30 min of treatment, showing consistently ultra-fast-killing kinetics as in the case of sterilizing active bacteria as well as dormant bacteria (Figure S17). Clearly, these results demonstrated **3a**'s superiority in treating persisters, a serious issue for many traditional antibiotics. This trait, combined with **3a**'s EPS penetration ability and disruption ability on the biofilm cell community, made this oligoamidine a fast-killing agent effective toward different types of bacterial cells in biofilms (Figure 4E,F).

Bacterial Membrane and DNA Dual-Targeting Antimicrobial Mechanism of 3a.

We next carried out the investigation of the nongrowth-related antimicrobial mechanism of **3a**, the prerequisite for killing persistent bacteria. To probe the affinity of **3a** binding to the bacterial cell membrane, we first measured the zeta potential of bacteria cells after treating **3a** at different concentrations. As shown in Figure 5A and Figure S18A, the surface of *S. aureus* and *E. coli* cells is negatively charged due to the presence of anionic lipids including cardiolipin, phosphatidylglycerol, phosphatidylinositol, teichoic acids

(for Gram-positive bacteria), and lipopolysaccharides (for Gram-negative bacteria), as major components of its phospholipid lipid bilayer.[55] With increasing concentration of **3a**, the zeta potential changed from negative to positive, suggesting effective binding of **3a** on the bacterial membrane. Such affinity of **3a** to the amphiphilic phospholipid lipid bilayer is granted by its alternatingly amphiphilic oligomeric structure, which also results in significant damage on the bacterial envelop, as imaged by SEM for active growing bacteria (Figure 5B) and dormant bacteria (Figure S18B). The membrane lysis caused by **3a** increased the cell permeability and allowed the entry of the membrane-impermeable propidium iodine dye, which gave fluorescence signals upon bacterial internalization and DNA binding (Figures 5C and S18C). This permeabilization effect also promotes the accumulation of additional **3a** in the bacterial cells that facilitates the binding to its second target, DNA. The *in vitro* DNA-binding activity of **3a** was first demonstrated by a gel retardance assay as well as a DNA dye competition assay, giving a dissociation constant of 5.3×10^{-9} M for DNA binding (Figures 5D,E and S18D). Next, the *in cellulo* DNA target of **3a** in bacterial cells was visualized with fluorescent confocal microscopy. As shown in Figure 5F, the genomic DNA of *A. b*-1 cells was stained with Hoechst (blue), and the bacterial cell membrane with Dio (green). Rhodamine-labeled **3a** (Rhod-**3a**, red, Figure S19) colocalized with both the Hoechst channel and the Dio channel, suggesting the spatial distribution of **3a** involving dual DNA and membrane colocalization. For a mammalian cell line 3T3, in contrast, Rhod-**3a** only concentrated in the cytoplasm without entering the nucleus and thus was void of DNA binding toxicity of mammalian cells (Figure 5F). This observed locational selectivity of DNA binding is attributed to the rod-like molecular shape granted by the rigid amphiphilic structure of **3a**, which facilitates internalization of bacterial cells via the interaction with phospholipids, and, on the other hand, ensures the exclusion of **3a** from the mammalian cell nuclear envelope, which has sieve-like properties.[56]

The combined membrane and DNA targeting modes of action have rendered **3a** strongly bactericidal with ultra-fast killing kinetics for active, dormant, and persister cells (Figures 4B–D and S17), as well as for the inhibition and eradication of biofilms (Figure 4E,F). Bactericidal antibiotics are also known to stimulate the production of toxic reactive oxygen species (ROS).[57] The ROS generation in **3a**-treated bacterial cells was indeed observed using a dichlorofluorescein diacetate (DCFHDA) probe and flow cytometry (Figures 5G and S18E). Thus, membrane disruption, DNA binding, and oxidation by ROS collectively cause remarkable and irreversible damage to the bacterial cells, resulting in the inability to generate resistance to **3a**. As shown in Figures 5H and S18F, **3a**-treated bacteria were free of resistance even after a three-week period. On the contrary, bacteria generated resistance against standard antibiotics from different classes (gentamicin from the aminoglycoside family and ampicillin from the β-lactam family) within a week.

Efficacy of 3a in *Ex Vivo* Models for Biofilm Infection.

Biofilm is an important source of bloodstream infection [58,59] (Figure 6A-i), tissue-related infections [60,61] (e.g., wound surface, Figure 6A-ii), and implant-related infections (Figure 6A-iii). An *ex vivo* bloodstream infection model was thus established to evaluate the ability of **3a** to eliminate biofilm from the blood and to protect red blood cells (RBCs) from lysis by the bacterial pathogen. Meanwhile, this study would also reveal whether toxicity concerns existed for this potent amphiphilic oligomer. The results shown in Figure 6B indicate that the infection with *S. aureus* at 2×10^6 CFU/mL results in bacterial proliferation to near 10^{10} CFU/mL density after 16 h, accompanied by complete lysis of the RBCs ("Control"). The treatment

with vancomycin had minimum effect on biofilm elimination and RBC rescue ("1 μg/mL vancomycin"), while the treatment with **3a** eradicated all *S. aureus* and, at the same time, completely rescued RBCs without introducing any hemolytic toxicity ("4 μg/mL **3a**", also in Figure S20).

We next evaluated **3a** with an *ex vivo* fibroblast biofilm infection model mimicking wound biofilm infection, which was the major cause of chronic wounds.[61] GFP-*S. aureus* adhere and colonize on the surface of the fibroblast as the initial step of biofilm formation, after which multilayered bacterial cells are profoundly accumulated, and enormous amounts of EPS are produced to form mature biofilms on the tissue, as shown in Figure 6C-i to Figure 6C-ii. It was also noted that the morphology of fibroblast cells was distorted upon infection with biofilm (Figure 6C-ii). The treatment with 8 μg/mL vancomycin was able to partially remove GFP-*S. aureus* biofilms, however, leaving patches of active bacterial lawn (Figure 6C-iii). The treatment with **3a** at the same concentration completely eliminated all bacteria from the cell surface and rescued the fibroblasts to their normal morphology (Figure 6C-iv). More quantitatively, a dose-dependent study with the fibroblast biofilm infection model suggests that **3a** has much more superior *ex vivo* anti-biofilm activity than vancomycin (Figure 6D).

Demonstration of the Anti-Biofilm Activity of a 3a-Grafted Polycaprolactone Surface.

Our *in vitro* and *ex vivo* results demonstrated that **3a** exhibited excellent performance in the antibacterial and anti-biofilm study. Thus, **3a** may also have a great potential to serve as a surface functionalization agent for implant devices to prevent biofilm formation, the major cause of implant-related complications leading to implant failure (Figure 6C-iii). To demonstrate this application, we attempted to graft **3a** onto the surface of polycaprolactone (PCL), which was a biodegradable polymer used in many FDA-approved surgical implants and drug delivery devices for tissue engineering and regenerative medicine applications.[62,63] PCL was first prepared via a standard electron-spin method [64] and the surface modification was performed via the previously reported procedures (Figure 7A).[41] Fourier transform infrared (FTIR) spectra characterization shown in Figure S21 provides evidence for grafting of **3a**. Morphology study with SEM suggests that the resulting **3a**-PCL thin film is composed of fibers with a diameter of $\sim$2 μm (Figures 7B and S22A). Moreover, the surface hydrophilicity analysis for pure PCL, PCL-COOH, and PCL-**3a** thin film shows that the addition of **3a** markedly enhanced the hydrophilicity of the PCL-**3a** thin film (Figure 7C). The contact angle of pure PCL thin film is 128.2 $\pm$ 3°, while the water droplet on the PCL-**3a** nanofiber surface is completely dispersed after 15 s. The increase in hydrophilicity originates from the amphiphilic characteristics of **3a** and may potentially result in a desirable anti-fouling effect because high hydrophilicity offers better anti-fouling resistance to most foulants that are commonly hydrophobic.[65] In addition, surface modifications with **3a** did not alter the original mechanical features of PCL (Figure S22B–E). Through the stability and anti-fouling test of the material, it can be observed that different pH conditions did not affect its anti-biofilm activities (Figure S23A), and compared with PCL, the anti-fouling ability of PCL-**3a** was also enhanced (Figure S23B).

To examine the antibacterial and anti-biofilm ability of the PCL-**3a** thin film, we adopted a protocol from the ISO22196 standard with modifications (Figure 7D). Briefly, 5×10^5/5×10^7 CFU/mL bacterial pathogens in PBS were applied to the surface of the material to mimic infection near the site of implant. After 2 or 24 h, an aliquot from the applied fluid was taken and then applied on an agar plate to determine the

antimicrobial effect for planktonic bacteria (Figure 7D-i). The thin film treated for 24 h was rinsed with PBS three times to remove free bacteria, and the amount of biofilm formation was determined by culturing the thin film on an agar plate (Figure 7D-ii). As shown in Figures 7E and S24, PCL-**3a** thin film not only effectively eliminated all planktonic *S. aureus* but also completely prevented the formation of biofilm on the surface. Additional experiments were performed with other bacterial pathogens prone to form biofilms on indwelling implants, namely, *P. a*, *K. pn*, *E. fa*, *A. b*, and *E. c*. PCL-**3a** thin film exhibited consistently a broad spectrum of antibacterial and anti-biofilm activity (Figures S22F and 7F). Furthermore, the hemocompatibility and cytotoxicity of PCL-**3a** thin films were examined (Figure 7G,H). The findings support that the material displays no observable toxicity in terms of RBC lysis or mammalian cell growth. Taken together, **3a** can be grafted onto the material surface, such as polycaprolactone, and the **3a**-modified surface shows strong antibacterial and anti-biofilm activities against a broad spectrum of pathogenic bacteria.

3a Displays a Strong Anti-Biofilm Efficacy in *In Vivo* Wound Biofilm Infection Models.

Encouraged by the promising results of **3a** against biofilms, we then evaluated the anti-biofilm activity of **3a** in mice wound models infected by *S. aureus* or *P. aeruginosa*, which were two of the most prevalent bacterial pathogens found in clinical biofilm-related diseases.[44,47,49,66] We first established a mice excisional wound model in which a large surface wound was artificially created in mice and the wound area was infected with a large amount of GFP-*S. aureus* (10^8 CFU) to allow biofilm formation,[67] as observed with NIR-II imaging (Figures 8A and S25A). During the study, mice were grouped, and their wound areas were treated with **3a** or PBS for 7 days, during which bacterial loads on wounds were determined and the status of mice, including the activity level, wound area, and body weight, was observed.

Notably, we observed that **3a** treatment resulted in 5-log reduction (for *S. aureus*) and 3-log reduction (for *P. aeruginosa*) of bacterial load on the wound surface after a 2-day treatment, indicating a significant improvement over the PBS group (Figures 8B,C and S25B). Moreover, **3a** treatment also promoted the healing of wounds, outperforming the PBS groups in achieving complete wound healing (Figure 8 D,E). It is noteworthy that the body weight of **3a**-treated mice increases normally and is comparable to that of the PBS group (Figure S25 C,D). In addition, the H&E staining section images showed that a 7-day treatment of **3a** did not induce any toxicity to the major organs (Figure S25E). *In vivo* toxicity was also evaluated with subcutaneous injection of **3a**, showing no effect on mouse body weight or body conditions (Figure S26). Taken together, **3a** displays a strong anti-biofilm efficacy in the mice excisional wound model with high biocompatibility.

CONCLUSIONS

In conclusion, a bifunctional oligoamidine (**3a**) with rigid alternatingly amphiphilic nature was developed and demonstrated for its high potency in the inhibition and eradication of biofilms of the most clinically important pathogenic bacteria, *P. aeruginosa*, *E. coli*, and *S. aureus*. The amphiphilic structure of the compound enabled the molecule to penetrate the amphiphilic and densely packed EPS so that it may disrupt the biofilm cell community. The cellular target of the compound was found be to bacterial membrane and DNA, which ensured **3a**'s bactericidal activity against dormant and persister bacteria.

Compared to antibiotics such as vancomycin, **3a** features much higher activity in biofilm inhibition and eradication, as well as bactericidal activity against dormant and persistent cells, demonstrating its effectiveness as an antibiofilm agent. Moreover, the fibroblast biofilm infection model indicated that the compound showed much better *ex vivo* antibiofilm activity than vancomycin, and with simple engineering methods, **3a** could be coated on the PCL surface potentially for convenient medical use. Most importantly, the compound exhibited a strong anti-biofilm efficacy in the mice excisional wound model with high biocompatibility and low *in vivo* cytotoxicity. As such, we believe that this bifunctional and dual-target oligoamidine, together with the SAR analysis, may reveal a new route toward solutions to the biofilm issue in medicinal chemistry and the development of novel medical devices.

METHODS

Materials and Instruments.

Materials. All solvents and reagents were purchased from Adamas Reagent (Shanghai, China), Sigma-Aldrich (USA), Macklin Chemical (Shanghai, China), and Leyan (Shanghai, China). Bio-reagents were purchased from Beyotime Biotechnology (Shanghai, China) unless noted otherwise. Reagents were used without further purification unless otherwise noted. Water was purified by a MilliQ water purification system. All solvents used were dried and stored over activated 4 Å molecular sieves.

Bacteria Strains and Cell Lines. The following bacteria were obtained from the American Type Culture Collection (ATCC, Manassas, VA): *S. aureus Newman strain* (ATCC 25904), *E. faecalis* (Andrewes and Horder) *Schleifer and Kilpper-Balz* (ATCC 19433), *K. pneumoniae* subsp. *pneumoniae Schroeter Trevisan* (ATCC 27736), *A. baumannii Bouvet and Grimont* (ATCC 19606), *P. aeruginosa* PA01 ((ATCC 47085), and *E. coli* K12 (ATCC 29425). *S. aureus* harbouring a GFP-expression plasmid (GFP-*Sa*) is a kind gift from Prof. Hang Xing from Hunan University. Bacterial clinical strains were provided by Dr. Kai Zhou from The First Affiliated Hospital of Southern University of Science and Technology, Dr. Hui Wang from the Department of Clinical Laboratories, Peking University People's Hospital, and Dr. Cuiyan Tan from the Department of Pulmonary and Critical Care Medicine Fifth Affiliated Hospital of Sun Yat-sen University. All bacteria strains were confirmed by 16S ribosomal DNA sequencing. Murine embryonic fibroblast cell line NIH/3T3 (ATCC CRL-1658) was purchased from ATCC.

Instrumentation.

Nuclear Magnetic Resonance. Nuclear magnetic resonance (NMR) spectra were recorded using a Bruker Avance II 400 MHz spectrometer equipped with an autosampler. The collected data were processed in MestReNova 6.1 and aligned/annotated in Adobe Illustrator CC.

Gel Permeation Chromatography. Gel permeation chromatography (GPC) analyses were performed on a Waters system equipped with a Waters 515 isocratic pump and a Waters 2414 refractive index detector. Separations were performed at 40 °C using an aqueous solution of $NaNO_3$ (0.01 M) as the mobile phase.

Matrix-Assisted Laser Desorption/Ionization-Time of Flight. The reaction products were detected by a 5800 MALDI-TOF/TOF (ABSciex) with reflective positive ion mode.

Flow Cytometry Study. All flow cytometry studies were performed on a Becton Dickinson Accuri C6 Plus instrument. The data obtained were processed in FlowJo, aligned, and annotated in Adobe Illustrator CC.

Dynamic Light Scattering Instrument. Changes in the particle size and zeta-potential analysis were observed on a Malvern Zetasizer Nano ZSP dynamic light scattering (DLS) instrument.

Confocal Microscopy. Fluorescence microscope images were acquired using a Nikon Eclipse Ti2-E Laser Confocal Microscope. For blue fluorescence, the wavelength was set at 405 nm for excitation. For green fluorescence, the wavelength was set at 488 nm for excitation. For red fluorescence, the wavelength was set at 561 nm for excitation.

Scanning Electron Microscopy. Scanning electron microscopy (SEM) experiments were conducted on a Hitachi S-4800 scanning electron microscope. Bacterial samples were gold-plated before image scanning on SEM.

Contact Angle Measurement. The wettability of nanofibers was evaluated by a Contact Angle Measuring System, model SEO Phoenix 300 Touch contact angle.

Synthesis of Amphiphilic Oligoamidines.

The synthetic route to the series of amphiphilic oligoamidines was referred to previous reports. Briefly, diethyl terephthalimidate dihydrochloride (1, 189.4 mg, 0.646 mmol, 1 equiv) and 1,3-bis(aminomethyl)benzene (2, 88 mg, 0.646 mmol, 1 equiv.) were mixed in 4 mL of anhydrous DMF in a 7 mL glass vial with a silicone-top screw cap under N2 protection. Then, triethylamine (TEA, 360.5 μL, 2.584 mmol, 4 equiv.) was added. The reaction was continuously stirred at 35 °C for 4 days. HCl(aq) (3.0 M, 2 mL) was added, and then, the solution was dialyzed (MWCO = 1 kDa) against water for 10 h and the water was replaced every 2 h. The purified solution was lyophilized to give **3a** as a white solid (155 mg). Except the synthesis using the diamine monomer, other listed oligomers were synthesized following the same procedures using the same equivalents for starting materials. NMR and GPC were used to characterize the amphiphilic oligoamidine synthesized.

For the labeling of **3a** with RhB/FITC, **3a** (10 mg) was added to phosphate buffer [(pH 8.5) 2 mL and 0.05 M]. Five micrograms RhB/FITC (excess) were dissolved in dimethyl sulfoxide (100 μL), and then, the solution was added to the solution of **3a**. The mixture was stirred for 2 h, and then, the concentrated HCl was carefully added to acidify the mixture to pH = 1. The resulting solution is a clear solution. To remove HCl and excess dyes, the solution was dialyzed using Spectra/Por 7 regenerated cellulose dialysis tubing (pretreated; MWCO = 1 kDa) against water for 10 h. The labeled **3a** was obtained in the solid form by freeze-drying in the dark.

Critical Micelle Concentration Measurements. A series of solutions from the concentration of 0−256 μg/mL was prepared in 200 μL of PBS (pH = 7.4), after which 5 μM Nile Red was added. The solution was incubated at 37 °C for 30 min and tested by a fluorescence spectrophotometer (excitation 550 nm, emission 570−750 nm). The fluorescence intensity at 650 nm was recorded and plotted.

Planktonic Bacteria-Related Assays.

MIC Measurement against Active Planktonic Bacteria. MIC was determined in CAMHB using the broth microdilution method according to the guidelines from the Clinical and Laboratory Standards Institute (CLSI). The MIC value was defined as the lowest concentration of a compound that inhibited bacterial growth by more than 90%. Bacteria were cultivated in CAMHB at 37 °C and 220 rpm overnight. The working solution containing bacteria was prepared at a concentration of 5×10^5 CFU/mL (5×10^7 CFU/mL for Figure 3B), and 100 μL of the solution was added into each well of a 96-well plate containing different concentrations of

the testing compound, and then, the plate was incubated at 37 °C and 220 rpm for 18−24 h. Solutions without bacteria were included in each plate as negative controls. MIC values were determined by reading the absorbance of the solution at 595 nm using a microplate reader. All assays were repeated in three independent experiments.

Antibacterial Activity Test for Dormant Bacteria in DMEM with 10% FBS. Log-phase culture of GFP-*Sa* was added to DMEM with 10% FBS at the concentration of 5×10^7 CFU/mL. The cells treated with **3a** or vancomycin were incubated at 37 °C and 220 rpm for 16−20 h. Bacterial load was determined through plating a 5 μL aliquot with a series of 10-fold dilution onto agar plates, and CFUs were counted after incubation for 10 h at 37 °C. Experiments were carried out in duplicate.

*Effect of **3a** on Persistent Bacteria.* Persistent GFP-*Sa* cells were generated following a previously reported protocol. Briefly, 6 mL of GFP-*Sa* cells at 1×10^8 CFU/mL was treated with vancomycin at a final concentration of 20 μg/mL, and then, they were incubated at 37 °C and 200 rpm for 6 h. At different time points, 10 μL aliquots were taken out for PBS dilution and CFU determination. At the end of vancomycin treatment, persistent GFP-*Sa* cells were collected by centrifugation and then resuspended with 6 mL of PBS. Different concentrations of **3a** were then added to the above culture, and bacterial loads were determined at different time points. Experiments were carried out in duplicate.

Killing Kinetics. Overnight culture of *E. coli* K12 and *S. aureus* was diluted in CAMHB (for active bacteria) or PBS (for dormant bacteria) to a final concentration of 2×10^6 CFU/mL. Set up of the assay was the same as the MIC measurement. Bacteria samples (5 μL) were collected from each treatment at the indicated time points during incubation. Samples were subsequently serially diluted in PBS, plated onto an LB agar plate, and incubated for 16 h before bacterial CFU determination. Experiments were carried out in duplicate.

Bacterial Biofilm-Related Assays.

Minimum Biofilm Inhibitory Concentration. GFP-*Sa* were cultured to the mid-logarithmic growth phase in CAMHB at 37 °C and 220 rpm and then were diluted in BM2 medium to 5×10^7 CFU/mL, as calculated and converted from the bacterial optical density at 595 nm. This suspension (100 μL) was added to each well of a 96-well polystyrene microplate. Solutions without bacteria were included in each plate as negative controls. Drugs were added to the wells, serially diluted, and incubated at 37 °C without agitation for 24 h (or the indicated time periods in the case of kinetic measurement) to allow biofilm formation. The suspension containing planktonic bacteria was then removed, and then, the wells were washed 3−4 times with 1× PBS to remove residual planktonic bacteria. Sterile 1× PBS (100 μL) was then added to each well containing bacterial biofilm. The biofilm was then dispersed with 15 min of ultrasound at 40 Hz (Branson). The released bacterial load was determined by plating serial tenfold dilutions on agar plates. The agar plates were then incubated overnight at 37 °C. The colonies were then quantified to determine bacteria CFU. MBIC was defined as the minimum concentration that inhibits the formation of biofilms. Experiments were carried out in duplicate.

MBEC against S. aureus Biofilm. GFP-*Sa* cells were cultured to the mid-logarithmic growth phase in CAMHB at 37 °C and 220 rpm and then were diluted in BM2 medium to 5×10^7 CFU/mL, as calculated and converted from the bacterial optical density at 595 nm. This suspension (100 μL) was added to each well of a 96-well polystyrene microplate. Solutions without bacteria were included in each plate as negative controls. Plates were incubated at 37 °C without agitation for 24 h to establish biofilm. After 24 h, the suspension containing

planktonic bacteria was removed, and the wells were washed 3−4 times with 1× PBS to remove residual planktonic bacteria. The drug solution was diluted to the desired concentration in BM2 medium by two-fold serial dilution and then was added into each well containing bacterial biofilm. Plates were incubated at 37 °C without agitation for 24 h (or the indicated time periods in the case of kinetic measurement). The colony counting method used was the same with that in MBIC. MBEC was defined as the minimum concentration that completely eradicates the mature biofilm. Experiments were carried out in duplicate.

MBICs and MBECs against P. aeruginosa and E. coli Biofilm. For measuring MBICs and MBECs against *P. aeruginosa* and *E. coli* biofilms, the experimental procedures for biofilm formation, inhibition, and eradication were the same as those of *S. aureus*, except for the use of biofilm-forming medium (Jensen's Medium for *P. aeruginosa* and M9 for *E. coli*). For final biofilm quantification, the liquid culture was first removed followed by the wells being washed with ddH_2O three times. Crystal violet (CV) solution (0.1%; 120 μL) was added to each well. The plates were incubated at 30 °C for approximately 30 min. Then, the CV solutions were removed, and the wells were washed with ddH_2O three times. Bacterial biofilms stained with CV were then quantified by dissolving CV with 40% acetic acid. The absorbance at 560 nm was measured with a microplate reader (MULTISKAN-MK3, THERMO Scientific). Experiments were carried out in duplicate.

*Labeling of **3a** Using RhB-ITC.* Rhodamine B isothiocyanate (2 mg) and 10 mg of **3a** dissolved in DMSO were stirred in water for 2 h, followed by the slow addition of hydrochloric acid for acidification. The solution was dialyzed and lyophilized away from light to obtain fluorescently labeled oligomer.

Fluorescence Microscopy and SEM Imaging of Biofilm

Formation and Disruption. The general protocols for MBIC and MBEC determination were applied, except that biofilm formation on a glass coverslip that was induced by placing the coverslip into a well of a sterile 24-well plate containing 1 mL of GFP-*Sa* at 5×10^7 CFU/ mL in BM2. After drug treatment, the glass coverslip was washed three to four times with PBS to remove planktonic bacteria.

For fluorescence microscopy imaging, the samples were imaged directly with inverted fluorescence microscopy or confocal fluorescence microscopy. For SEM imaging, biofilms formed on the glass coverslip were fixed with 2% glutaraldehyde overnight at 4 °C. The samples were then dehydrated with a series of ethanol solutions (30, 50, 70, 90, and 100% in Milli-Q purified water) and sputter-coated with gold for observation using a Hitachi S-4800 field emission scanning electron microscope.

Imaging of 3D Biofilms. Fluorescence microscope images were acquired using a Nikon Eclipse Ti2-E Laser Confocal Microscope. For blue fluorescence, the wavelength was set at 405 nm for excitation. For green fluorescence, the wavelength was set at 488 nm for excitation. For red fluorescence, the wavelength was set at 561 nm for excitation. The fluorescent and differential interference contrast (DIC) images were acquired with an FV1000 confocal laser scanning microscope (Olympus, Japan) The biofilm biomass and thickness were quantified by COMSTAT software.

Toxicity-Related Assays.

Hemolytic Activity Test. Whole sheep blood was diluted to a 4% blood working suspension by PBS, followed by addition into a 96-well plate and treatment with **3a**. After being incubated for 1 h at 37 °C without agitation, the microplate was centrifuged at 300 g for 10 min. Aliquots of the supernatant were then transferred to a clear 96-well plate and the OD595 was measured by a plate reader. The untreated RBCs

and 150 μL working suspension with 4% Triton were used as negative and positive controls, respectively. Experiments were carried out in duplicate. The percentage of hemolysis was obtained by the following formula:

$$\%\text{Hemolysis} = \left[\frac{\text{OD}_{\text{sample}} - \text{OD}_{\text{neg}}}{\text{OD}_{\text{pos}} - \text{OD}_{\text{neg}}}\right] \times 100$$

Membrane Disruption Mechanism.

Under Growth Conditions. The overnight cultured *E. coli* K12 (USA) and *S. a* cells were diluted 20 times to 5 mL by CAMHB in culture tubes (OD595 = 0.05). The cells were treated with the drug of interest for 4 h. The sample without treatment served as a control. The samples were pelleted down at 1500 g for 10 min, then fixed with 2% glutaraldehyde overnight. Next, the samples were dehydrated using a series of ethanol solutions. After being lyophilized, the samples were mounted on a copper tape, air-dried, and sputter-coated with gold for observation using a Hitachi S-4800 field emission scanning electron microscope.

Under Nongrowth Conditions. The overnight cultured *E. coli* K12 (USA) was obtained by centrifugation at 1500 g for 5 min at room temperature and washed 3 times with PBS. Then, the collected cells were diluted to OD = 0.25 with PBS and treated with the drug of interest for 4 h. The following steps were the same as those described in "Under growth conditions."

Zeta Potential Measurement. The overnight culture of *S. a* or *E. coli* K12 cell was washed and then diluted with HEPES (40 mM, pH 7.4) to a final concentration of OD595 = 0.1. Different concentrations of **3a** were added into the bacteria suspension. The mixtures were incubated at 37 °C and 220 rpm for 2 h. Zeta potentials were measured on a Malvern Zetasizer Nano ZSP zetasizer. Experiments were carried out in duplicate.

*Effect of **3a** on Bacterial Membrane Permeability.* Propidium iodide was used as the fluorescent dye to evaluate the integrity of bacterial membranes. A stationary-state culture of *E. coli* was washed three times with PBS and then resuspended to OD595 = 0.2 containing 100 μM PI. The samples were treated by **3a** and incubated at 37 °C for 3 h. Cells were then analyzed via flow cytometry (Accuri C6 Plus, Becton Dickinson) using a 488 nm laser source. Red fluorescence emitted by propidium iodide was detected on FL2-PE. In all cases, 10,000 events were counted. Experiments were carried out in duplicate.

DNA Binding Mechanism. *Gel Retardation Assay.* Plasmid pCold-ctx-m-15 (20 μg/mL) was incubated with different concentrations of **3a** at 37 °C for 30 min. After incubation, the mixture was running on a 1% agarose gel with Gel-Red (2 μg/mL) for 1 h. The DNA band shifts were visualized under ultraviolet. The *K*d value for Gel-Red is 5.6×10^{-8} M.

Hoechst Competition Assay. A Hoechst competition assay was used to quantify the DNA-binding affinity of **3a**. The experiment was performed in PBS (pH 7.4) at 25 °C. eDNA (10 μg/mL) and 4 μg/mL Hoechst were added to a 200 μL centrifuge tube. Then, different concentrations of **3a** were introduced into the centrifuge tubes. The final volume was 200 μL. The solution was mixed and incubated at 37 °C for 30 min. The process was monitored by a fluorescence spectrometer. Experiments were carried out in duplicate. The *K*d value

determined for Hoechst is 5.6 × 10^{-8} M. The *K*i value determined for **3a**-DNA interactions is calculated as follows:

$$K_i = \frac{IC_{50}}{1 + \frac{[ligand]}{K_d}}$$

Selectively Binding DNA in Bacterial Nucleoids. Rhodamine B isothiocyanate (RhB-ITC) was used to label **3a** to obtain fluorescently labeled **3a**-RhB. **3a**-RhB (8 μg/mL) was incubated with NIH/3T3 cells in DMEM supplemented with 10% FBS for 24 h or with *A. baumannii*-1 in PBS for 2 h. The medium was then removed, and the cells were washed three times with PBS. The bacteria were stained in PBS with Hoechst (5 μg/mL) for 15 min and followed with DiO (10 μM) for 20 min. The cells were then stained in PBS with Hoechst (5 μg/mL) for 30 min at 37 °C. After the bacteria and cells were washed three times with PBS, 1 mL of 4% paraformaldehyde fixing solution was added. The resulting cultures were incubated for 30 min at 37 °C. Finally, paraformaldehyde was replaced with an appropriate amount of PBS after washing three times with PBS. Samples were imaged with a Nikon A1R MP confocal microscope. The distribution of the drug in the cells and bacteria was analyzed by co-localization of green (DiO), blue (Hoechst), and red (**3a**-RhB) fluorescence.

ROS Generation and Resistance Evolution.

ROS Detection and Quantification. E. coli K12 was cultured overnight in 5 mL of CAMHB at 37 °C. The bacterial cells were then washed three times and resuspended in PBS. The suspension was diluted to OD595 = 0.2 and mixed with 5 μM DCFH-DA to prepare a working solution. The working solution was then added into a 96-well plate (200 μL per well) and treated with different concentrations of **3a** for 3 h at 37 °C in the dark. The ROS analysis was performed immediately by flow cytometry (*E*x = 488 nm ± 30 nm, *E*m = 533 ± 30 nm). Experiments were carried out in duplicate.

Resistance Generation Assay. The method for multistep resistance evolution was adapted from a reported procedure.46 Briefly, the broth microdilution method for MIC determination against *E. coli* K12 or *S. a* was repeated for 16 or 27 passages over a period of 16 days (for *E. coli*) or 27 days (for *S. a*). The initial inoculum was 5 × 10^5 CFU/mL in CAMHB. For each subsequent passage, the inoculum for MIC determination was adjusted to a final density of approximately 5 × 10^5 CFU/mL using the contents of a well containing **3a**, ampicillin, or gentamicin at a subinhibitory concentration (at which the bacterial growth was observed from the previous passage). To measure the MIC of each passage, bacteria were transferred to a new 96-well microtiter plate. Compounds were then added (in triplicate) to the wells in the first row of the microtiter plate and then serially diluted. The plate was incubated at 37 °C for a minimum of 24 h before the MIC was determined by reading OD595 values. Resistance was identified as greater than a 4-fold increase compared to the initial MIC. Experiments were carried out in duplicate.

***Ex Vivo* Model of Biofilm Infection.**

RBC-Bacterium Co-Culture Model. Log-phase culture (2 × 10^6 CFU/mL) of GFP-*Sa* was added to PBS with 4% sheep red blood cells (RBCs). The cells treated with **3a** were incubated at 37 °C and 220 rpm for 16−20 h. Bacterial load was determined through plating a 5 μL aliquot with a series of 10-fold dilution onto agar plates and CFUs were counted after 10 h incubation at 37 °C. Experiments were carried out in duplicate.

Fibroblast Biofilm Infection Model. The experiment was performed by following the previously reported protocols.[68,69] A total of 5 × 104 NIH/3T3 cells were cultured in Dulbecco's modified Eagle medium (DMEM) with 10% FBS at 37 °C in a humidified atmosphere of 5% CO_2. Cells were maintained for 24 h to reach a confluent monolayer. Bacteria (GFP-*Sa*) were inoculated and harvested as mentioned above. Afterward, seeding solutions with 5 × 10^7 cells/mL were inoculated in buffered DMEM supplemented with 10% FBS. The original medium was removed from 3T3 cells followed by addition of 100 μL of seeding solution. The cocultures were then stored in a box humidified with damp paper towels at 37 °C overnight without shaking. Then, the original medium was removed from 3T3 cells and replaced with serially diluted drugs. The cocultures were then stored in a box humidified with damp paper towels at 37 °C overnight without shaking. After 24 h, imaging was performed with an inverted fluorescence microscope. The free bacterial solution was removed, and the wells were washed 3−4 times with 1× PBS to remove planktonic bacteria. The bacteria were then resuspended in 100 μL of sterile 1× PBS. After 15 min of ultrasound at 40 Hz (Branson), the dispersed biofilm bacteria were counted by plating serials of tenfold dilutions on agar plates. Agar plates were incubated overnight at 37 °C, and colonies were quantified to determine bacteria CFU. Solutions without bacteria were included in each plate as negative controls. Experiments were carried out in duplicate.

In Vivo Mouse Model of Biofilm Infection.

Anti-Biofilm Efficacy Evaluation on the Mice Excision Wound Model. All animal procedures were performed in accordance with the Guidelines for Care and Use of Laboratory Animals of Hunan University with license number SYXK-2018-0006 and approved by the Animal Ethics Committee of China. The protocol was established based on previously reported protocols.[67] Adult male ICR mice (6−8 weeks old, ∼20 g) were anesthetized with an intraperitoneal injection of chloral hydrate (50 mg/kg), and one open excision wound (2∼3 cm^2) was created to the depth of loose subcutaneous tissue on the dorsal side skin for each mouse. A suspension of *P. aeruginosa* clinical isolate or *S. aureus* (10^8 CFU) was inoculated on the excision wound area to establish the infection. For the *S. a* infection experiment, mice were separated into two groups: the PBS-treatment group (*N* = 9) and the **3a**-treatment group (20 mg/kg, *N* = 9). For the *P. a* infection experiment, mice were separated into two groups: the PBS-treatment group (*N* = 3) and the **3a**-treatment group (20 mg/kg, *N* = 3). Treatments were started 24 h after infection by applying the drug of interest to the wound area and were repeated every day for 7 days. Bacterial loads on the wound were determined. The status of mice, including the activity level, wound area, and body weight, was observed and recorded daily.

*Toxicity Evaluation with Subcutaneous Injection of **3a**.* This animal study was performed in accordance with national regulations on animal studies. Eight ICR mice (adult male, 6−8 weeks old, weighing ∼30 g) were divided into 2 groups: the control group (PBS, *N* = 4) and the subcutaneous injection group (10 mg/kg, *N* = 4). Mice were treated with **3a** in ddH_2O via subcutaneous injection for 7 days. The body weight was monitored for each mouse daily.

PCL-3a Thin-Film-Related Experiments.

Preparation of the Membrane. The polycaprolactone (PCL) nanofiber membrane was fabricated by electrospinning. Briefly, 0.5 g of PCL powder was dissolved in a mixed solvent system (1.5 mL of anhydrous ethanol and 3.5 mL of DCM) with the aid of ultrasonication. The solution was stirred at room temperature

for 6 – 12 h. The nanofiber membranes were fabricated using commercially available electrospinning equipment (JDF05 Changsha Nanoapparatus Co., Ltd., China). The above solution was transferred into a 10 mL plastic syringe attached to a capillary tip with an inner diameter of 0.9 mm (yellow) and pumped out at a rate of 0.5 – 2 mL/h. An electric potential of 20 – 25 kV was supplied to the metal needles to form charged liquid jets that, upon rapid evaporation of the solvent, turned into nanofibers on the collector of the instrument (the distance between the capillary tip and the fiber collector was 15 cm). All of the nanofibers were deposited on the nonwoven substrate (15 cm × 15 cm) that overlaid on a grounded metal roller (diameter of 12 cm) rotated at a speed of 50 rpm. To guarantee uniform membrane morphology, the injection pump was set to move horizontally backward and forward at a speed of 20 cm/min over a distance of 2 cm. The temperature and relative humidity in the laboratory were 25 ± 2 °C and 40 ± 2%, respectively.

*Surface Modification of the PCL Membrane with **3a**.* The PCL material was soaked with 1 M NaOH(aq) for 3 – 4 h, rinsed with deionized water 3 – 4 times, and then soaked with 80 mg/mL 1-(3-dimethylaminopropyl)-3-ethylcarbodiimide hydrochloride (EDC) and 5 mg/mL **3a** for 6 – 12 h to obtain **3a**-modified PCL (**3a**-PCL).

Biofilm Imaging on Materials. GFP-*Sa* (100 μL 5 × 10^7 CFU/mL) was dropped to the surface of the 1 × 1 cm^2 material in a 24-well plate and cultured at 37 °C for 24 h. Then, the material was rinsed with PBS, fixed with paraformaldehyde, and observed with confocal microscopy for formation of GFP-*S. a* biofilm.

SEM of Membranes. The average diameter and morphology of the electrospun nanofibers were characterized using a Hitachi S-4800 scanning electron microscope at an accelerating voltage of 20 kV. Samples of nanofibers were coated with a 5 nm thick layer of gold using a sputter coater (Bal-Tec, MD20 instrument). The nanofiber diameters were calculated by the ImageJ software (*n* = 50).

Contact Angle Measurement. The wettability of the electrospun nanofibers was evaluated by a Contact Angle Measuring System, model SEO Phoenix 300 Touch contact angle. The nanofibers were placed on a sample stand and water was dropped onto their surface to measure the contact angles. A camera was used to record the image of the drop. The average contact angle was obtained using Surfaceware9 software.

*Stability Test of PCL-**3a**.* PCL-**3a** (1 × 1 cm^2) was rinsed with PBS and soaked in different solutions (ddH_2O with pH = 4, 6, 8, or 10) for 24 h or Protease K for 2 h. The treated material was placed in a 24-well plate; after that, 100 μL of 5 × 10^5 CFU/mL *S. a* was dropped on the surface of the material. The surface planktonic bacteria was sampled and diluted for CFU determination after incubation at 37 °C for 24 h.

*Antifouling Test of PCL-**3a**.* Antifouling properties of PCL and PCL-**3a** were evaluated by the stander BSA rejection method.[70] BSA adsorption of the membranes was evaluated using the method of Bradford according to the standard protocol of the Bio-Rad protein assay. Each 1 × 1 cm^2 PCL or PCL-**3a** was rinsed with 20 mL of ethanol for 30 min and then with 20 mL of PBS for another 30 min. The membrane was next soaked in 5 mL of 0.01 M PBS solution with 0.1 mg/mL BSA at 37 °C. Protein concentration in solution was determined by reading OD595 at different time points (1, 3, 5, 7, 21, and 24 h).

Antimicrobial Testing with Membranes. The protocol for surface antimicrobial testing for planktonic bacteria was adapted from International standard ISO 22196 (Plastics_Measurement of antibacterial activity on plastics surfaces). Briefly, 60 μL of test inoculum containing 5 × 10^7 CFU/mL bacteria was transferred to the test surface with a dimension of 1 cm × 1 cm. The sample was incubated at 37 °C with relative humidity >90% for 24 h. Then, 5 μL of bacterial solution was sampled after 24 h for CFU determination to quantify the bactericidal effect on planktonic bacteria. For measuring biofilm formation

on the test surface, the material was washed with sterile PBS 3 times to remove the planktonic bacteria. The material was then incubated on LB solid medium with the test surface downward at 37 °C for 16∼24 h. Then, bacterial growth around the test material was observed. Experiments were carried out in duplicate.

Material Hemolytic Activity Test. PCL-**3a**, PCL-NaOH, and plain PCL were irradiated under UV lamp for 10 min, cut into 1 × 1 cm^2, and placed separately in wells of a 24-well plate. One milliliter of 4% fresh sheep blood in PBS was added to each well containing the material, and the 24-well plate was placed in a 37 °C incubator for 2 h without agitation. After that, the RBC working solution was transferred into a 1.5 mL centrifuge tube and centrifuged at 300 g for 10 min. The supernatant (100 μL) was then transferred to a clean 96-well plate. The absorbance was read at 576 nm with a microplate reader. In the experiment, the sample treated with 4% Triton X-100 was used as a fully lysed control and the untreated working solution was used as a negative control. Experiments were carried out in duplicate.

Material Cytotoxicity. The NIH/3T3 cells were inoculated into 24-well plates with 1 × 10^4 cells in each well and cultured in an incubator containing 5% CO_2 at 37 °C for 24 h to promote adhesion. Then, the cells were treated with PCL-**3a**, PCL-NaOH, and PCL (1 × 1 cm^2) for 24 h in DMEM-10% FBS. The wells without material treatment were used as control. After incubation, the medium and material were removed. The cells were then washed with PBS once, and 120 μL of fresh medium containing 0.5 mg/mL MTT was added. The cells were cultured at 37 °C and in 5% CO_2 atmosphere for 1.5 h. The cell viability was determined by measuring the absorbance at 595 nm with 100 μL of DMSO as the alternative medium. Experiments were carried out in duplicate. The cell survival rate was expressed as a percentage and calculated as follows:

$$\text{viability}\% = \text{Abs}_{595\ \text{nm}}\ \text{of treated sample} / \text{Abs}_{595\ \text{nm}}\ \text{of control} \times 100\%$$

ACKNOWLEDGMENTS

X.F. thanks Prof. Hang Xing (Hunan University), Dr. Kai Zhou (The First Affiliated Hospital of Southern University of Science and Technology), Dr. Hui Wang (Peking University People's Hospital), and Dr. Cuiyan Tan (Fifth Affiliated Hospital of Sun Yat-sen University) for providing bacterial strains. The funding support from the National Natural Science Foundation of China (Grants 22177031 to X.F., 21877033 and 92163127 to Y.B., 82102415 to M.W., 21874038 to Q.C.), the Natural Science Foundation of Hunan Province (2021JJ30088 to Y.B., 2021JJ40055 to M.W.), the Research Grants Council of the Hong Kong Special Administrative Region, China (RGC Project No. 15300522 to W.W.), and the Fundamental Research Funds for the Central Universities (531118010738 to C. H.) are gratefully acknowledged.

REFERENCES

(1) Bjarnsholt, T.; Jensen, P. O.; Moser, C.; Hoiby, N. *Biofilm Infections*; Springer, 2011.

(2) Jamal, M.; Ahmad, W.; Andleeb, S.; Jalil, F.; Imran, M.; Nawaz, M. A.; Hussain, T.; Ali, M.; Rafiq, M.; Kamil, M. A. Bacterial Biofilm and Associated Infections. *J. Chin. Med. Assoc.* 2018, *81*, 7−11.

(3) Veerachamy, S.; Yarlagadda, T.; Manivasagam, G.; Yarlagadda, P. K. D. V. Bacterial Adherence and Biofilm Formation on Medical Implants: A Review. *Proc. Inst. Mech. Eng., Part H* 2014, *228*, 1083−1099.

(4) Lewis, K. Riddle of Biofilm Resistance. *Antimicrob. Agents Chemother.* 2001, *45*, 999−1007.

(5) Karygianni, L.; Ren, Z.; Koo, H.; Thurnheer, T. Biofilm Matrixome: Extracellular Components in Structured Microbial Communities. *Trends Microbiol.* 2020, *28*, 668−681.
(6) Epstein, A. K.; Pokroy, B.; Seminara, A.; Aizenberg, J. Bacterial Biofilm Shows Persistent Resistance to Liquid Wetting and Gas Penetration. *Proc. Natl. Acad. Sci. U. S. A.* 2011, *108*, 995−1000.
(7) Arnaouteli, S.; MacPhee, C. E.; Stanley-Wall, N. R. Just in Case It Rains: Building a Hydrophobic Biofilm the Bacillus Subtilis Way. *Curr. Opin. Microbiol.* 2016, *34*, 7−12.
(8) Kobayashi, K.; Iwano, M. Bsla(Yuab) Forms a Hydrophobic Layer on the Surface of Bacillus Subtilis Biofilms. *Mol. Microbiol.* 2012, *85*, 51−66.
(9) Hobley, L.; Ostrowski, A.; Rao, F. V.; Bromley, K. M.; Porter, M.; Prescott, A. R.; MacPhee, C. E.; van Aalten, D. M. F.; Stanley-Wall, N. R. Bsla Is a Self-Assembling Bacterial Hydrophobin That Coats the *Bacillus Subtilis* Biofilm. *Proc. Natl. Acad. Sci. U. S. A.* 2013, *110*, 13600−13605.
(10) Zeng, G.; Vad, B. S.; Dueholm, M. S.; Christiansen, G.; Nilsson, M.; Tolker-Nielsen, T.; Nielsen, P. H.; Meyer, R. L.; Otzen, D. E. Functional Bacterial Amyloid Increases Pseudomonas Biofilm Hydrophobicity and Stiffness. *Front. Microbiol.* 2015, *6*, 1099.
(11) Cucarella, C.; Solano, C.; Valle, J.; Amorena, B.; Lasa, I.; Penades, J. R. Bap, a Staphylococcus Aureus Surface Protein Involved in Biofilm Formation. *J. Bacteriol.* 2001, *183*, 2888−2896.
(12) Tursi, S. A.; Tukel, C. Curli-Containing Enteric Biofilms inside and Out: Matrix Composition, Immune Recognition, and Disease Implications. *Microbiol. Mol. Biol. Rev.* 2018, *82*, e00028−e00018.
(13) Taglialegna, A.; Navarro, S.; Ventura, S.; Garnett, J. A.; Matthews, S.; Penades, J. R.; Lasa, I.; Valle, J. Staphylococcal Bap Proteins Build Amyloid Scaffold Biofilm Matrices in Response to Environmental Signals. *PLoS Pathog.* 2016, *12*, No. e1005711.
(14) Quan, K.; Hou, J.; Zhang, Z.; Ren, Y.; Peterson, B. W.; Flemming, H. C.; Mayer, C.; Busscher, H. J.; van der Mei, H. C. Water in Bacterial Biofilms: Pores and Channels, Storage and Transport Functions. *Crit. Rev. Microbiol.* 2022, *48*, 283−302.
(15) Pinto, R. M.; Soares, F. A.; Reis, S.; Nunes, C.; Van Dijck, P. Innovative Strategies toward the Disassembly of the Eps Matrix in Bacterial Biofilms. *Front. Microbiol.* 2020, *11*, 952.
(16) Ceri, H.; Olson, M. E.; Stremick, C.; Read, R. R.; Morck, D.; Buret, A. The Calgary Biofilm Device: New Technology for Rapid Determination of Antibiotic Susceptibilities of Bacterial Biofilms. *J. Clin. Microbiol.* 1999, *37*, 1771−1776.
(17) Lebeaux, D.; Ghigo, J.-M.; Beloin, C. Biofilm-Related Infections: Bridging the Gap between Clinical Management and Fundamental Aspects of Recalcitrance toward Antibiotics. *Microbiol. Mol. Biol. Rev.* 2014, *78*, 510−543.
(18) Koo, H.; Allan, R. N.; Howlin, R. P.; Stoodley, P.; Hall-Stoodley, L. Targeting Microbial Biofilms: Current and Prospective Therapeutic Strategies. *Nat. Rev. Microbiol.* 2017, *15*, 740−755.
(19) Verderosa, A. D.; Totsika, M.; Fairfull-Smith, K. E. Bacterial Biofilm Eradication Agents: A Current Review. *Front. Chem.* 2019, *7*, 824.
(20) Joseph, R.; Naugolny, A.; Feldman, M.; Herzog, I. M.; Fridman, M.; Cohen, Y. Cationic Pillararenes Potently Inhibit Biofilm Formation without Affecting Bacterial Growth and Viability. *J. Am. Chem. Soc.* 2016, *138*, 754−757.

(21) Etayash, H.; Qian, Y.; Pletzer, D.; Zhang, Q.; Xie, J.; Cui, R.; Dai, C.; Ma, P.; Qi, F.; Liu, R.; Hancock, R. E. W. Host Defense Peptide-Mimicking Amphiphilic Beta-Peptide Polymer (Bu:Dm) Exhibiting Anti-Biofilm, Immunomodulatory, and in Vivo Anti-Infective Activity. *J. Med. Chem.* 2020, *63*, 12921−12928.

(22) Vishwakarma, A.; Dang, F.; Ferrell, A.; Barton, H. A.; Joy, A. Peptidomimetic Polyurethanes Inhibit Bacterial Biofilm Formation and Disrupt Surface Established Biofilms. *J. Am. Chem. Soc.* 2021, *143*, 9440−9449.

(23) Thuy-Khanh, N.; Lam, S. J.; Ho, K. K. K.; Kumar, N.; Qiao, G. G.; Egan, S.; Boyer, C.; Wong, E. H. H. Rational Design of Single-Chain Polymeric Nanoparticles That Kill Planktonic and Biofilm Bacteria. *ACS Infect. Dis.* 2017, *3*, 237−248.

(24) Han, X.; Lou, Q.; Feng, F.; Xu, G.; Hong, S.; Yao, L.; Qin, S.; Wu, D.; Ouyang, X.; Zhang, Z.; Wang, X. Spatiotemporal Release of Reactive Oxygen Species and No for Overcoming Biofilm Heterogeneity. *Angew. Chem., Int. Ed.* 2022, *61*, No. e202202559.

(25) Ho, D.-K.; Murgia, X.; De Rossi, C.; Christmann, R.; de Mello, H.; Martins, A. G.; Koch, M.; Andreas, A.; Herrmann, J.; Mueller, R.; Empting, M.; Hartmann, R. W.; Desmaele, D.; Loretz, B.; Couvreur, P.; Lehr, C.-M. Squalenyl Hydrogen Sulfate Nanoparticles for Simultaneous Delivery of Tobramycin and an Alkylquinolone Quorum Sensing Inhibitor Enable the Eradication of *P Aeruginosa* Biofilm Infections. *Angew. Chem., Int. Ed.* 2020, *59*, 10292−10296.

(26) Guo, S.; Huang, Q.; Chen, Y.; Wei, J.; Zheng, J.; Wang, L.; Wang, Y.; Wang, R. Synthesis and Bioactivity of Guanidinium-Functionalized Pillar 5 Arene as a Biofilm Disruptor. *Angew. Chem., Int. Ed.* 2021, *60*, 618−623.

(27) Zhou, C.; Wang, Y. Structure-Activity Relationship of Cationic Surfactants as Antimicrobial Agents. *Curr. Opin. Colloid Interface Sci.*2020, *45*, 28−43.

(28) Vu, B.; Chen, M.; Crawford, R. J.; Ivanova, E. P. Bacterial Extracellular Polysaccharides Involved in Biofilm Formation. *Molecules* 2009, *14*, 2535−2554.

(29) Slomberg, D. L.; Lu, Y.; Broadnax, A. D.; Hunter, R. A.; Carpenter, A. W.; Schoenfisch, M. H. Role of Size and Shape on Biofilm Eradication for Nitric Oxide-Releasing Silica Nanoparticles. *ACS Appl. Mater. Interfaces* 2013, *5*, 9322−9329.

(30) Yu, L.; Li, K.; Zhang, J.; Jin, H.; Saleem, A.; Song, Q.; Jia, Q.;Li, P. Antimicrobial Peptides and Macromolecules for Combating Microbial Infections: From Agents to Interfaces. *ACS Appl. Bio Mater.* 2022, *5*, 366−393.

(31) Siedenbiedel, F.; Tiller, J. C. Antimicrobial Polymers in Solution and on Surfaces: Overview and Functional Principles. *Polymer* 2012, *4*, 46−71.

(32) Locock, K. E.; Michl, T. D.; Valentin, J. D.; Vasilev, K.; Hayball, J. D.; Qu, Y.; Traven, A.; Griesser, H. J.; Meagher, L.; Haeussler, M. Guanylated Polymethacrylates: A Class of Potent Antimicrobial Polymers with Low Hemolytic Activity. *Biomacromolecules* 2013, *14*, 4021−4031.

(33) Ding, X.; Duan, S.; Ding, X.; Liu, R.; Xu, F.-J. Versatile Antibacterial Materials: An Emerging Arsenal for Combatting Bacterial Pathogens. *Adv. Funct. Mater.* 2018, *28*, No. 1802140.

(34) Blackman, L. D.; Qu, Y.; Cass, P.; Locock, K. E. S. Approaches for the Inhibition and Elimination of Microbial Biofilms Using Macromolecular Agents. *Chem. Soc. Rev.* 2021, *50*, 1587−1616.

(35) Dey, R.; Mukherjee, S.; Barman, S.; Haldar, J. Macromolecular Nanotherapeutics and Antibiotic Adjuvants to Tackle Bacterial and Fungal Infections. *Macromol. Biosci.* 2021, *21*, No. e2100182.
(36) Ghosh, S.; Mukherjee, S.; Patra, D.; Haldar, J. Polymeric Biomaterials for Prevention and Therapeutic Intervention of Microbial Infections. *Biomacromolecules* 2022, *23*, 592−608.
(37) Pranantyo, D.; Zhang, K.; Si, Z.; Hou, Z.; Chan-Park, M. B. Smart Multifunctional Polymer Systems as Alternatives or Supplements of Antibiotics to Overcome Bacterial Resistance. *Biomacromolecules* 2022, *23*, 1873−1891.
(38) Si, Z.; Zheng, W.; Prananty, D.; Li, J.; Koh, C. H.; Kang, E. T.; Pethe, K.; Chan-Park, M. B. Polymers as Advanced Antibacterial and Antibiofilm Agents for Direct and Combination Therapies. *Chem. Sci.* 2022, *13*, 345−364.
(39) Bai, S. L.; Wang, J. X.; Yang, K. L.; Zhou, C. L.; Xu, Y. F.; Song, J. F.; Gu, Y. X.; Chen, Z.; Wang, M.; Shoen, C.; Andrade, B.; Cynamon, M.; Zhou, K.; Wang, H.; Cai, Q. Y.; Oldfield, E.; Zimmerman, S. C.; Bai, Y. G.; Feng, X. X. A Polymeric Approach toward Resistance-Resistant Antimicrobial Agent with Dual-Selective Mechanisms of Action. *Sci. Adv.* 2021, *7*, No. abc9917.
(40) Chen, Z.; Zhou, C.; Xu, Y.; Wen, K.; Song, J.; Bai, S.; Wu, C.; Huang, W.; Cai, Q.; Zhou, K.; Wang, H.; Wang, Y.; Feng, X.; Bai, Y. An Alternatingly Amphiphilic, Resistance-Resistant Antimicrobial Oligoguanidine with Dual Mechanisms of Action. *Biomaterials* 2021, *275*, No. 120858.
(41) Chen, Z.; Zhang, W.; Chen, Y.; Wang, Y.; Bai, S.; Cai, Q.; Pu, H.; Wang, Z.; Feng, X.; Bai, Y. Alternatingly Amphiphilic Antimicrobial Oligoguanidines: Structure−Property Relationship and Usage as the Coating Material with Unprecedented Hemocompatibility. *Chem. Mater.* 2022, *34*, 3670−3682.
(42) Huang, G.; Shen, H.; Chen, X.; Wu, T.; Chen, Z.; Chen, Y.; Song, J.; Cai, Q.; Bai, Y.; Pu, H.; Feng, X. A Degradable, Broad-Spectrum and Resistance-Resistant Antimicrobial Oligoguanidine as a Disinfecting and Therapeutic Agent in Aquaculture. *Polym. Chem.* 2022, *13*, 3539−3551.
(43) Roy, R.; Tiwari, M.; Donelli, G.; Tiwari, V. Strategies for Combating Bacterial Biofilms: A Focus on Anti-Biofilm Agents and Their Mechanisms of Action. *Virulence* 2018, *9*, 522−554.
(44) David, M. Z.; Daum, R. S. Community-Associated Methicillin-Resistant Staphylococcus Aureus: Epidemiology and Clinical Consequences of an Emerging Epidemic. *Clin. Microbiol. Rev.* 2010, *23*, 616−687.
(45) Richter, M. F.; Drown, B. S.; Riley, A. P.; Garcia, A.; Shirai, T.; Svec, R. L.; Hergenrother, P. J. Predictive Compound Accumulation Rules Yield a Broad-Spectrum Antibiotic. *Nature* 2017, *545*, 299−304.
(46) Song, J. F.; Malwal, S. R.; Baig, N.; Schurig-Briccio, L. A.; Gao, Z. J.; Vaidya, G. S.; Yang, K. L.; Abutaleb, N. S.; Seleem, M. N.; Gennis, R. B.; Pogorelov, T. V.; Oldfield, E.; Feng, X. X. Discovery of Prenyltransferase Inhibitors with in Vitro and in Vivo Antibacterial Activity. *ACS Infect. Dis.* 2020, *6*, 2979−2993.
(47) Gordon, R. J.; Lowy, F. D. Pathogenesis of Methicillin-Resistant Staphylococcus Aureus Infection. *Clin. Infect. Dis.* 2008, *46*, S350−S359.
(48) Beloin, C.; Roux, A.; Ghigo, J. M. Escherichia Coli Biofilms. *Curr Top Microbiol Immunol.* 2008, *322*, 249−289.
(49) Mulcahy, L. R.; Isabella, V. M.; Lewis, K. Pseudomonas Aeruginosa Biofilms in Disease. *Microb. Ecol.* 2014, *68*, 1−12.
(50) Sauer, K.; Stoodley, P.; Goeres, D. M.; Hall-Stoodley, L.; Burmolle, M.; Stewart, P. S.; Bjarnsholt, T. The Biofilm Life Cycle: Expanding the Conceptual Model of Biofilm Formation. *Nat. Rev. Microbiol.* 2022, 608.

(51) Lewis, K. Persister Cells, Dormancy and Infectious Disease. *Nat. Rev. Microbiol.* 2007, *5*, 48−56.
(52) Stokes, J. M.; Yang, K.; Swanson, K.; Jin, W.; Cubillos-Ruiz, A.; Donghia, N. M.; MacNair, C. R.; French, S.; Carfrae, L. A.; Bloom-Ackerman, Z.; Tran, V. M.; Chiappino-Pepe, A.; Badran, A. H.;Andrews, I. W.; Chory, E. J.; Church, G. M.; Brown, E. D.; Jaakkola, T. S.; Barzilay, R.; Collins, J. J. A Deep Learning Approach to Antibiotic Discovery. *Cell* 2020, *180*, 688.
(53) Kohanski, M. A.; Dwyer, D. J.; Collins, J. J. How Antibiotics Kill Bacteria: From Targets to Networks. *Nat. Rev. Microbiol.* 2010, *8*, 423−435.
(54) Fisher, R. A.; Gollan, B.; Helaine, S. Persistent Bacterial Infections and Persister Cells. *Nat. Rev. Microbiol.* 2017, *15*, 453−464.
(55) Silhavy, T. J.; Kahne, D.; Walker, S. The Bacterial Cell Envelope. *Cold Spring Harbor Perspect. Biol.* 2010, *2*, No. a000414.
(56) Paine, P. L.; Moore, L. C.; Horowitz, S. B. Nuclear Envelope Permeability. *Nature* 1975, *254*, 109−114.
(57) Kohanski, M. A.; Dwyer, D. J.; Hayete, B.; Lawrence, C. A.; Collins, J. J. A Common Mechanism of Cellular Death Induced by Bactericidal Antibiotics. *Cell* 2007, *130*, 797−810.
(58) Bryers, J. D. Medical Biofilms. *Biotechnol. Bioeng.* 2008, *100*, 1−18.
(59) Srinivasan, R.; Santhakumari, S.; Poonguzhali, P.; Geetha, M.; Dyavaiah, M.; Xiangmin, L. Bacterial Biofilm Inhibition: A Focused Review on Recent Therapeutic Strategies for Combating the Biofilm Mediated Infections. *Front. Microbiol.* 2021, *12*, No. 676458.
(60) Lebeaux, D.; Chauhan, A.; Rendueles, O.; Beloin, C. From in Vitro to in Vivo Models of Bacterial Biofilm-Related Infections. *Pathogens* 2013, *2*, 288−356.
(61) Percival, S. L.; McCarty, S. M.; Lipsky, B. Biofilms and Wounds: An Overview of the Evidence. *Adv. Wound Care* 2015, *4*, 373−381.
(62) Samuel Chackalamannil, D. R.; Ward, S. E. *Comprehensive Medicinal Chemistry III*; Elsevier, 2017.
(63) Narayan, R. *Encyclopedia of Biomedical Engineering*, 1st ed.; Elsevier, 2018.
(64) Xi, Y.; Ge, J.; Guo, Y.; Lei, B.; Ma, P. X. Biomimetic Elastomeric Polypeptide-Based Nanofibrous Matrix for Overcoming Multidrug-Resistant Bacteria and Enhancing Full-Thickness Wound Healing/Skin Regeneration. *ACS Nano* 2018, *12*, 10772−10784.
(65) Kumar, R.; Ismail, A. F. *Fouling Control on Microfiltration/Ultrafiltration Membranes: Effects of Morphology, Hydrophilicity, and Charge*. 2015, *132* (21), 42042, DOI: 10.1002/app.42042.
(66) Boucher, H. W.; Corey, G. R. Epidemiology of Methicillin-Resistant Staphylococcus Aureus. *Clin. Infect. Dis.* 2008, *46*, S344−S349.
(67) Hoque, J.; Konai, M. M.; Sequeira, S. S.; Samaddar, S.; Haldar, J. Antibacterial and Antibiofilm Activity of Cationic Small Molecules with Spatial Positioning of Hydrophobicity: An in Vitro and in Vivo Evaluation. *J. Med. Chem.* 2016, *59*, 10750−10762.
(68) Gupta, A.; Landis, R. F.; Li, C.-H.; Schnurr, M.; Das, R.; Lee, Y.-W.; Yazdani, M.; Liu, Y.; Kozlova, A.; Rotello, V. M. Engineered Polymer Nanoparticles with Unprecedented Antimicrobial Efficacy and Therapeutic Indices against Multidrug-Resistant Bacteria and Biofilms. *J. Am. Chem. Soc.* 2018, *140*, 12137−12143.
(69) Diaconu, A.; Coenye, T.; Barboiu, M.; Vincent, S. P. Dynamic Constitutional Frameworks as Antibacterial and Antibiofilm Agents. *Angew. Chem., Int. Ed.* 2021, *60*, 22505−22512.

(70) Chen, Z.; Du, X.-A.; Liu, Y.; Ju, Y.; Song, S.; Dong, L. A High-Efficiency Ultrafiltration Nanofibrous Membrane with Remarkable Antifouling and Antibacterial Ability. *J. Mater. Chem. A* 2018, *6*, 15191−15199.

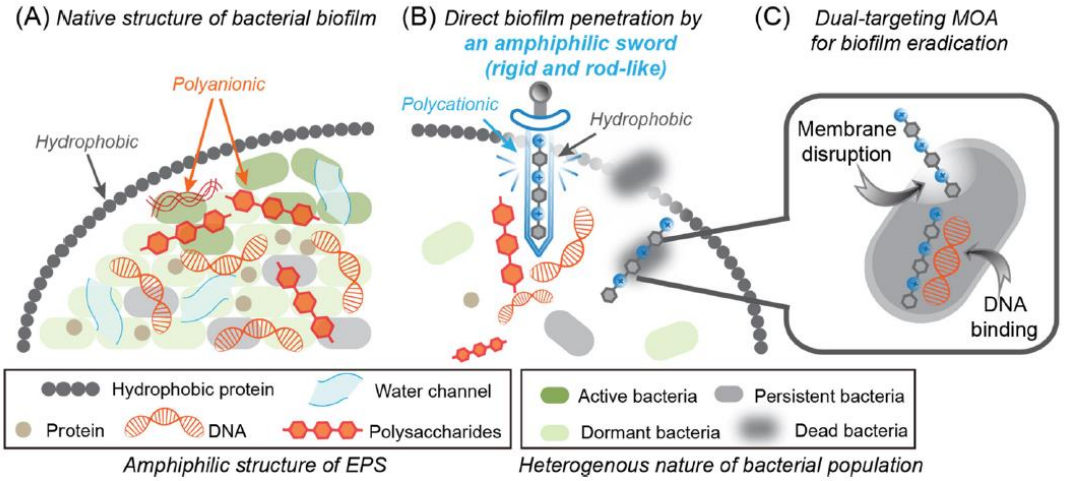

Figure 1. Design of amphiphilic oligomers for inhibition and eradication of bacterial biofilms. (A) Structure of biofilm with emphasis on the intrinsic characteristics of biofilm, namely, the amphiphilic structure of EPS and the heterogenous nature of the bacterial population. (B) Alternatingly amphiphilic oligomers developed to enhance biofilm penetration and combat dormant bacteria. (C) Oligomers display the bacterial membrane-DNA dual-targeting mechanism.

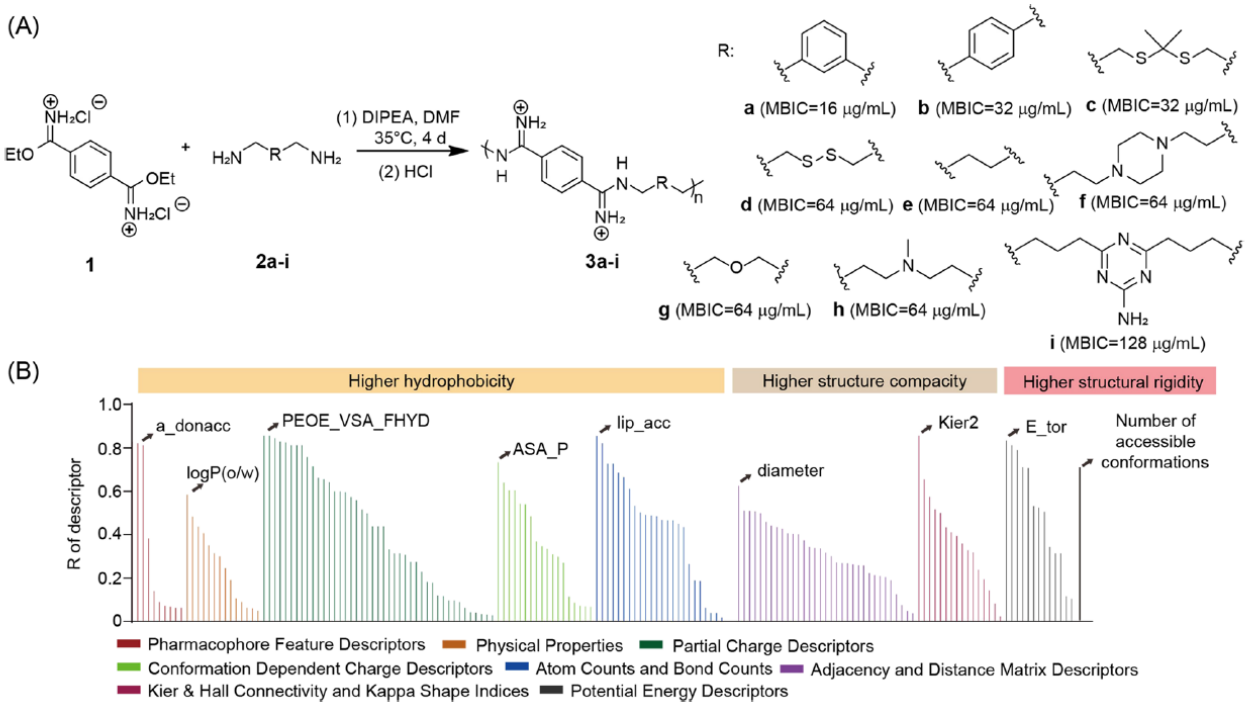

Figure 2. Development of an oligoamidine library for bacterial biofilm inhibition. (A) Synthesis of a series of amphiphilic oligoamidines, together with their MBICs against *S. aureus* biofilm (in parenthesis). (B) Top 9 best descriptors for the inhibition of biofilm formation screening showed that hydrophobicity, structural compactness, and rigidity were the key determinants in inhibiting biofilm formation.

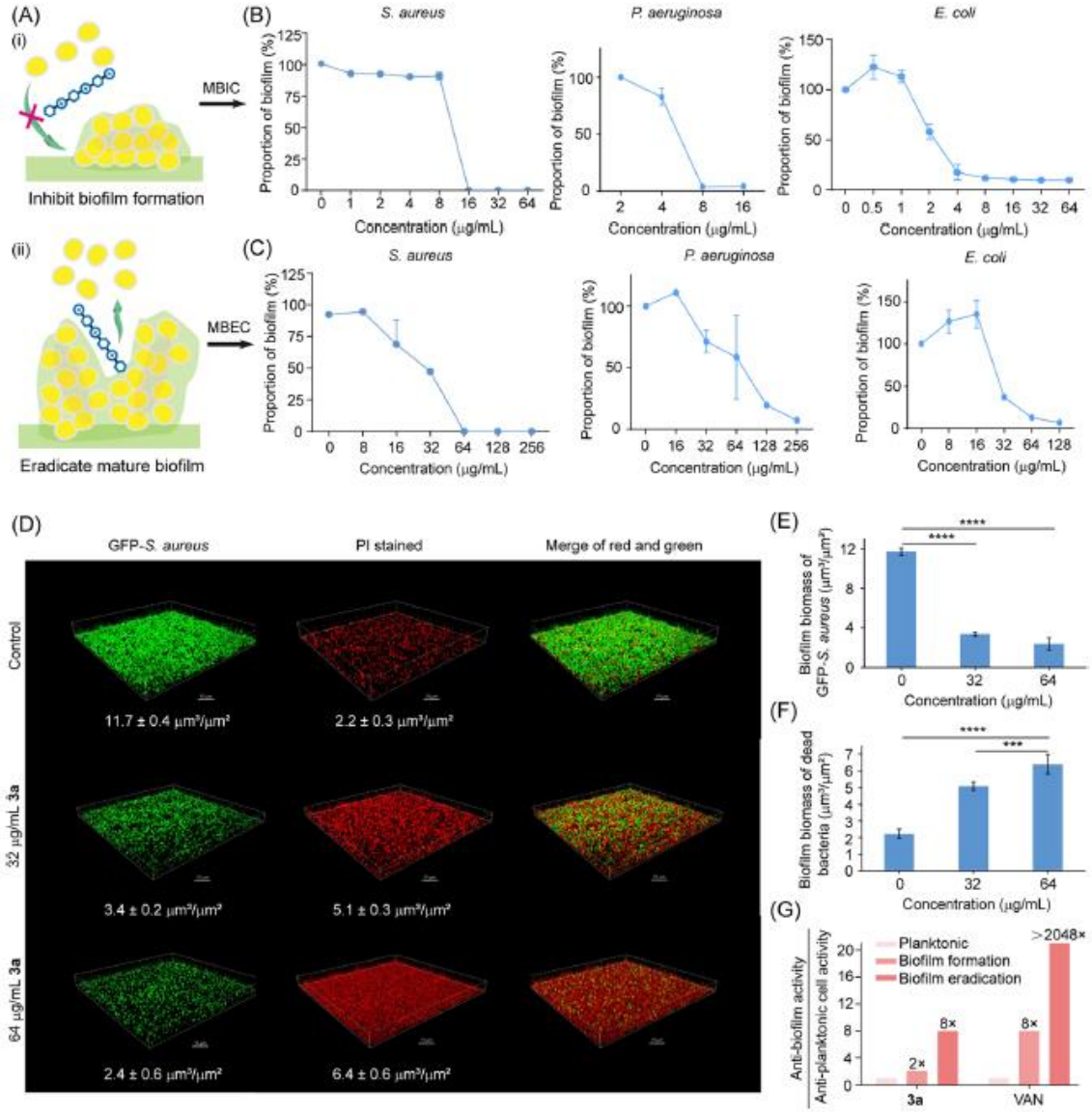

Figure 3. 3a effectively inhibited biofilm formation and disrupted mature biofilms formed by various bacterial pathogens. (A) Schematic representation of (i) biofilm inhibition and (ii) eradication. (B) Dose-dependent effects for the inhibition of biofilm formation with **3a** against GFP-*S. aureus*, *P. aeruginosa*, and *E. coli*. The proportion of biofilm was defined as the amount of biofilm after treatment divided by the initial amount of biofilm. (C) Dose-dependent effects for the eradication of mature biofilms with **3a** against GFP-*S. aureus*, *P. aeruginosa*, and *E. coli*. (D) 3D fluorescence confocal micrographs of mature GFP-*Sa* biofilms treated with **3a** (32 and 64 μg/mL). Propidium iodide (PI) stains dead bacteria within the biofilm. (E,F) Quantification of GFP-*S. aureus* biofilm and dead bacteria in Figure 3D. (G) Activity comparison of **3a** and vancomycin against planktonic, dormant, and persistent bacteria.

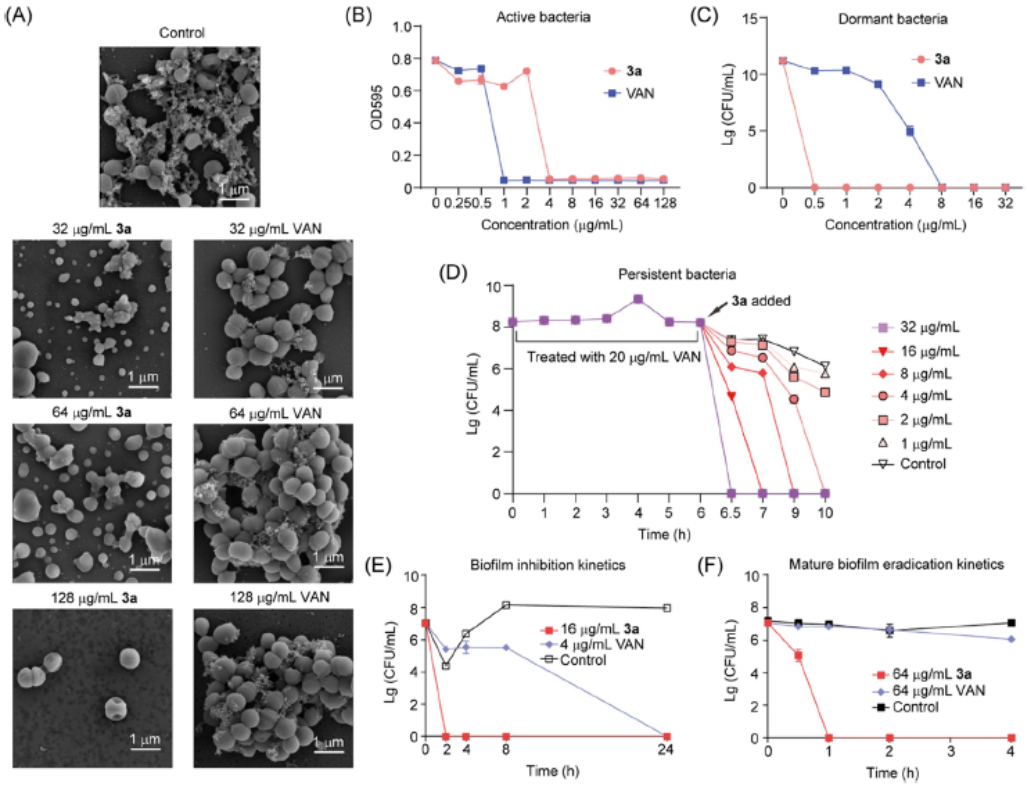

Figure 4. 3a disrupts the biofilm cell community and kills bacteria with different lifestyles. (A) Microscopic visualization of eradication activity of 3a and vancomycin against GFP-*Sa* biofilm by SEM. (B) Killing activity of 3a at different concentrations against active bacteria (GFP-*Sa*) cultured in CAMHB. (C) Killing activity of 3a at different concentrations against dormant bacteria (GFP-*Sa*) cultured in DMEM+10% FBS. (D) Killing kinetics of 3a at different concentrations against GFP-*Sa* persister cells produced by vancomycin treatment. (E) Biofilm inhibition kinetics of 3a and vancomycin against GFP-*Sa*. (F) Biofilm disrupting kinetics of 3a and vancomycin against GFP-*Sa*. VAN: vancomycin.

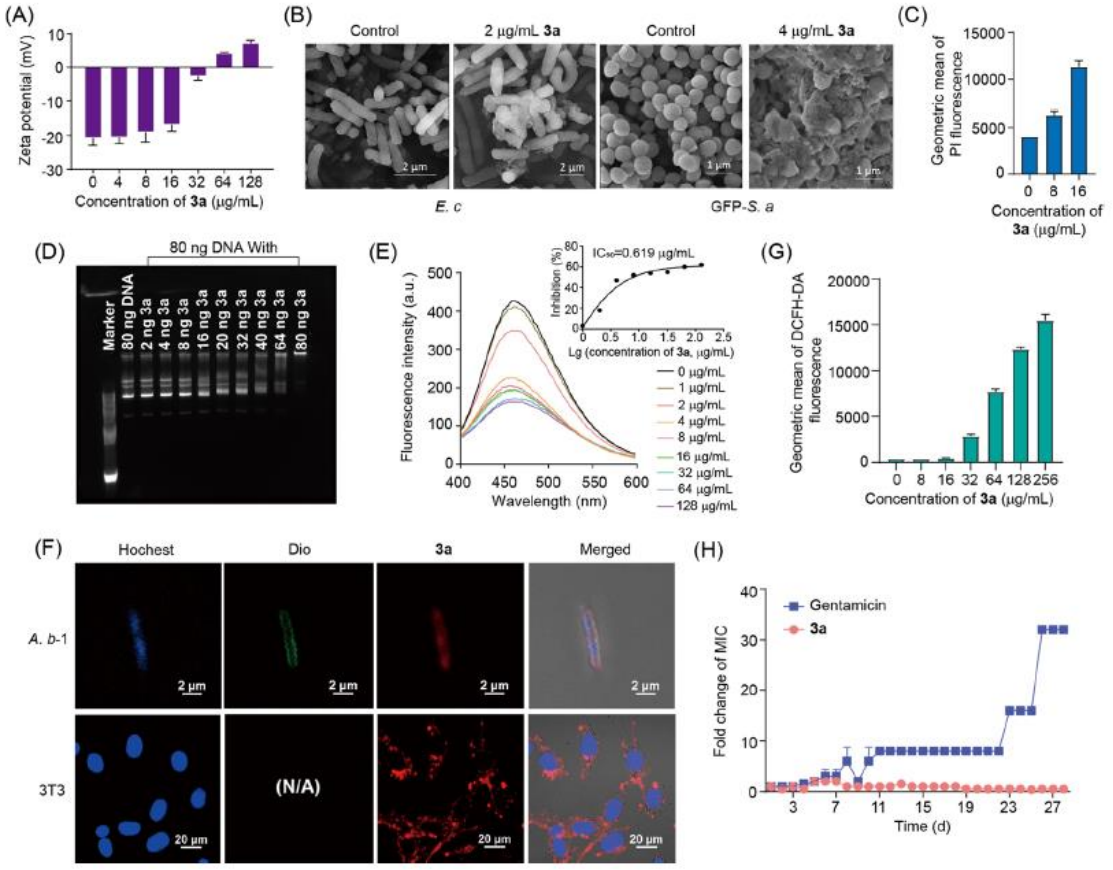

Figure 5. Bacterial membrane and DNA dual-targeting antimicrobial mechanism of 3a. (A) Zeta potential changes of bacteria cells after being treated with 3a at different concentrations. (B) 3a-treated *E. coli* (K12) (left) and GFP-*Sa* (right) cells under growth conditions showing membrane damage, exhibiting fragments and wrinkled surfaces. (C) Membrane permeability assays of *E. coli* cells with propidium iodide staining to demonstrate the bacterial cell membrane disruption caused by the addition of 3a. (D) Gel retardation assays to show the complexation of a 6500-bp plasmid DNA (Pcold-ctxm-15) with 3a. The DNA used was fluorescently labeled by Gel-Red. (E) Fluorophotometric studies to show the displacement of the minor groove binding dye by 3a. In the assays, Hoechst 33342 was bound to double-stranded DNA (dsDNA) and displaced by 3a. (F) Confocal microscopic images showed that 3a stained both the cell membrane and genomic DNA of *A. baumannnii*-1. 3a enters eukaryotic cells (NIH/3T3) but cannot pass through the nuclear membrane into the nucleus. (G) ROS response of *E. coli* treated with 3a at different concentrations. DCFH-DA was used as the ROS probe to indicate the cellular ROS level. (H) Comparison of the resistance generation rate of gentamicin and 3a against *S. aureus*.

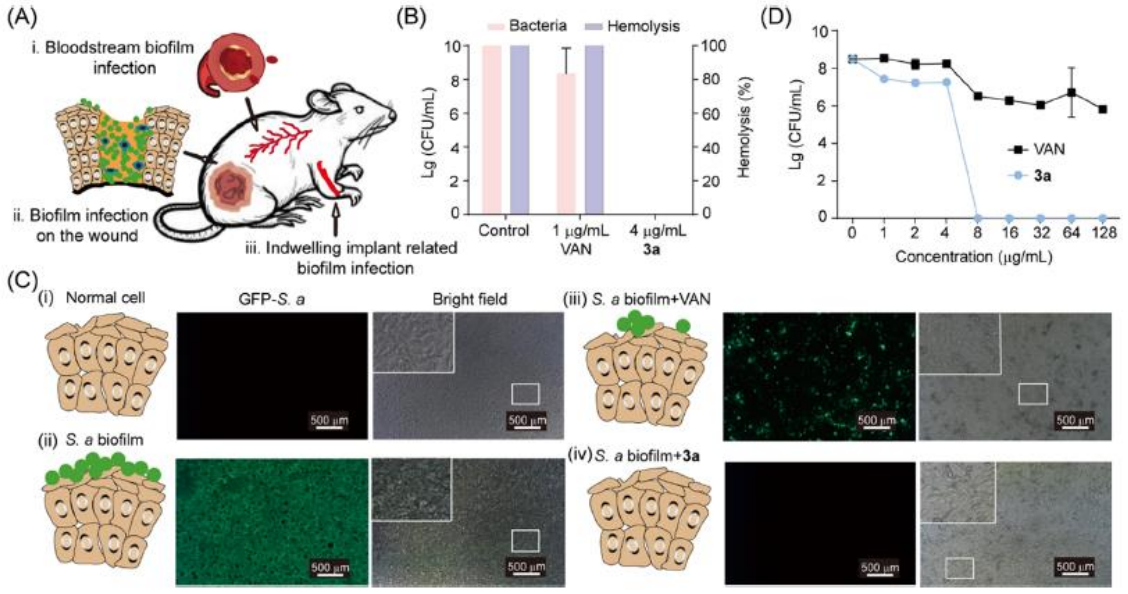

Figure 6. Antibacterial effects of 3a in both ex vivo and in vivo infection models. (A) Diagram of biofilm infection in the bloodstream, on the wound, and on implant devices. (B) Rescue of GFP-*Sa* bacteria-infected RBCs by 3a. 3a showed better performance than vancomycin in killing GFP-*Sa* in the presence of RBCs without causing hemolysis. (C) Confocal images for the antibiofilm effect of 3a (8 μg/mL) and vancomycin (8 μg/mL) with an ex vivo fibroblast biofilm infection model based on an NIH-3T3 cell line. (D) Dose-dependent effects of 3a and vancomycin in the fibroblast biofilm infection model.

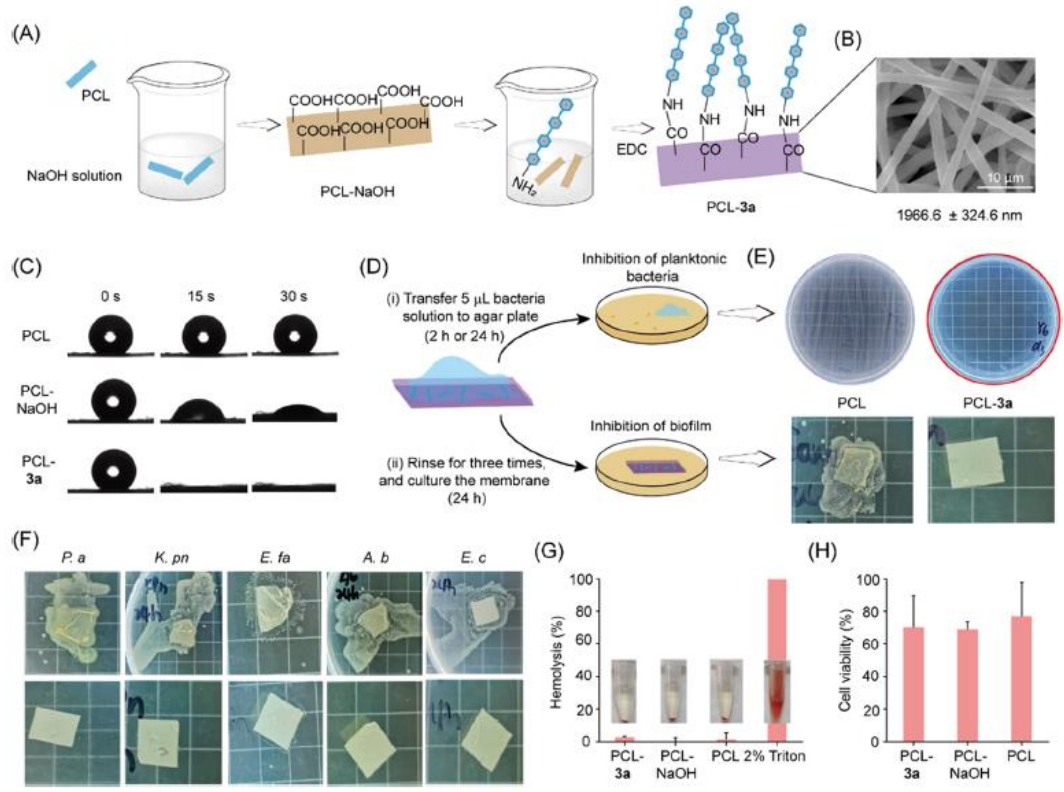

Figure 7. Preparation and antimicrobial testing of the 3a-grafted polycaprolactone surface. (A) Schematic diagram of the synthesis of a 3a-grafted polycaprolactone (PCL) membrane. (B) SEM images of the PCL-3a nanofibrous matrix. (C) Contact angle measurements for water droplets on various matrix surfaces at different time points. (D) Scheme of antibacterial and antibiofilm testing for the PCL surface. (E) Effects of PCL and PCL-3a membrane against planktonic *S. aureus* and its biofilm formation. (F) Antibiofilm effects of PCL and PCL-3a membranes against different biofilm-forming bacteria. (G) Hemolytic toxicity analysis of RBCs after incubation with different materials and chemicals. (H) Viability of NIH/3T3 cells after being cultured with different materials.

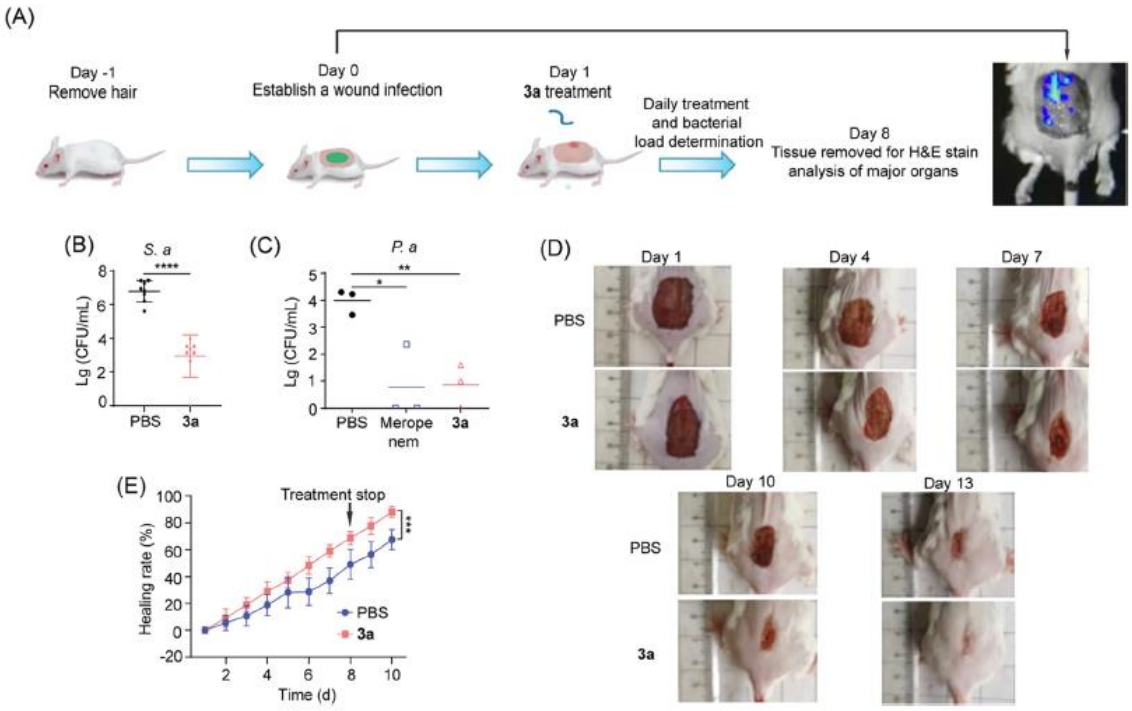

Figure 8. Efficacy of 3a in in vivo wound biofilm infection models. (A) Schematic overview of the biofilm-infected excision wound model and the NIR-II image of the *S. a* biofilm-infected wound on mice. (B,C) Effects of 3a in reducing the bacterial biofilm load on the wounds. (D) Representative images of excision wound healing of mice in the *S. aureus* infected model. (E) Effect of 3a in enhancing the wound healing rate in the *S. aureus* infected mice.